Human Dicer helicase domain recruits PKR and dsRNA binding proteins during viral infection

Thomas Montavon, Morgane Baldaccini, Mathieu Lefèvre, Erika Girardi, Béatrice Chane-Woon-Ming, Mélanie Messmer, Philippe Hammann, Johana Chicher, Sébastien Pfeffer

Human Dicer helicase domain recruits PKR and dsRNA binding proteins during viral infection

Thomas C. Montavon[1,*], Morgane Baldaccini[1,*], Mathieu Lefèvre[1,*], Erika Girardi[1], Béatrice Chane-Woon-Ming[1], Mélanie Messmer[1], Philippe Hammann[2], Johana Chicher[2], Sébastien Pfeffer[1,‡]

[1] Université de Strasbourg, Architecture et Réactivité de l'ARN, Institut de Biologie Moléculaire et Cellulaire du CNRS, 2 allée Konrad Roentgen, 67084 Strasbourg France

[2] Université de Strasbourg, Institut de Biologie Moléculaire et Cellulaire du CNRS, Plateforme Protéomique Strasbourg – Esplanade, 2 allée Konrad Roentgen, 67084 Strasbourg France

*These authors contributed equally

‡ To whom correspondence should be addressed: spfeffer@unistra.fr

Abstract

The antiviral innate immune response mainly involves type I interferon (IFN) in mammalian cells. The contribution of the RNA silencing machinery remains to be established, but several recent studies indicate that the ribonuclease DICER can generate viral siRNAs in specific conditions. It has also been proposed that type I IFN and RNA silencing could be mutually exclusive antiviral responses. In order to decipher the implication of DICER during infection of human cells with the Sindbis virus, we determined its interactome by proteomics analysis. We show that DICER specifically interacts with several double-stranded RNA binding proteins and RNA helicases during viral infection. In particular, proteins such as DHX9, ADAR-1 and the protein kinase RNA-activated (PKR) are enriched with DICER in virus-infected cells. We demonstrate the importance of DICER helicase domain in its interaction with PKR and showed that it has functional consequences for the cellular response to viral infection.

Introduction

In mammalian cells, the main antiviral defense system involves the activation of a signaling cascade relying on production of type I interferon (IFN I). This pathway depends on the recognition of extrinsic signals or pathogen associated molecular patterns (PAMPs) by dedicated host receptors. Double-stranded (ds) RNA, which can originate from viral replication or convergent transcription, is a very potent PAMP and can be sensed in the cell by various proteins among which a specific class of DExD/H-box helicases called RIG-I-like receptors (RLRs) (Ivashkiv and Donlin, 2014). RLRs comprise RIG-I, MDA5 and LGP2 and transduce viral infection signals to induce expression of IFN I cytokines that act in autocrine and paracrine fashion. These cytokines then trigger the expression of hundreds of interferon stimulated genes (ISGs) to stop the virus in its tracks (Borden et al, 2007). Among those ISGs, dsRNA-activated protein kinase R (PKR) plays an important role in antiviral defense by blocking cellular and viral translation upon direct binding to long dsRNA (Williams, 1999). PKR is a serine-threonine kinase that dimerizes and auto-phosphorylates upon activation. It then phosphorylates numerous cellular targets among which the translation initiation factor eIF2α, which results in the inhibition of cap-dependent translation (Lemaire et al., 2008). Accordingly, translation of many RNA viruses, including alphaviruses, is inhibited by PKR (Fros and Pijlman, 2016; Pfaller et al., 2011; Ryman et al., 2002). PKR is also involved in other cellular pathways including apoptosis, autophagy and cell cycle (Kim et al., 2014; Williams, 1999).

RNAi is another evolutionary conserved pathway triggered by long dsRNA sensing (Meister and Tuschl, 2004). One key component in this pathway is the type III ribonuclease DICER, which is also essential for micro (mi)RNA biogenesis (Hutvágner et al., 2001; Wienholds et al., 2003). These small regulatory RNAs are sequentially produced by the two ribonucleases DROSHA and DICER, before being loaded into an Argonaute (AGO) effector protein in order to regulate their target mRNAs (Bartel, 2018). Whatever its substrate, be it long

dsRNA or miRNA precursor, DICER relies on interacting with co-factors to be fully functional. In mammalian cells, the TAR-RNA binding protein (TRBP), a dsRNA binding protein (dsRBP), was shown to play a role in the selection of DICER substrates, its stabilization, strand selection and incorporation into AGO2 (Chendrimada et al., 2005). The interaction with TRBP is well characterized and depends on the helicase domain of DICER and the third dsRNA binding domain (dsRBD) of TRBP (Daniels et al., 2009). Another dsRBP, the protein activator of interferon-induced protein kinase R (PACT), was also described as an important cofactor of DICER. Although its function is not fully understood, PACT seems to also participate in miRNA loading and strand selection (Heyam et al., 2015; Kok et al., 2007) *via* protein-protein interaction between the DICER helicase domain and the third dsRBD of PACT (Lee et al., 2006).

It is now common knowledge that RNAi is the main antiviral defense system in several phyla such as plants, arthropods and nematodes (reviewed in (Guo et al., 2019)). However, its exact contribution in the mammalian antiviral response remains unclear (Cullen, 2006; Maillard et al., 2019; tenOever, 2016). Recent studies indicate that a functional antiviral RNAi does exist in mammals in specific cases. A functional antiviral RNAi response was first detected in undifferentiated mouse embryonic stem cells (Maillard et al., 2013) lacking the IFN response, suggesting that these two pathways could be incompatible. Indeed, in mammalian somatic cells deficient for MAVS or IFNAR, two components of the interferon response, an accumulation of DICER-dependent siRNAs derived from exogenous long dsRNA was detected (Maillard et al., 2016). In addition, the RLR LGP2 was found interacting with both DICER and TRBP, blocking respectively siRNA production and miRNA maturation (Takahashi et al., 2018a, 2018b; van der Veen et al., 2018). Moreover, AGO4 was recently shown to be involved in antiviral RNAi against Influenza A virus (IAV), Vesicular stomatitis virus (VSV) and Encephalomyocarditis virus (EMCV) (Adiliaghdam et al., 2020). Finally, viral suppressors of RNAi (VSRs) have been

shown to prevent DICER from playing an antiviral role in mammalian cells (Qiu et al., 2017, 2020). Nonetheless, several studies reported no detection of viral siRNAs in mammalian somatic cells infected with several viruses (Girardi et al., 2013; Parameswaran et al., 2010; Schuster et al., 2019). In somatic cells, only a helicase-truncated form of human DICER could produce siRNAs from IAV genome (Kennedy et al., 2015), but it also turned out that these siRNAs cannot confer an antiviral state (Tsai et al., 2018).

Based on these conflicting observations, we decided to study the involvement of DICER during infection of human cells with the Sindbis virus (SINV). SINV is a member of the *Togaviridae* family in the alphavirus genus, which is transmitted by mosquitoes to mammals and can induce arthritogenic as well as encephalitic diseases (Griffin, 2007). It is widely used as a laboratory alphaviruses model as it infects several cell types and replicates to high titers. SINV has a positive stranded RNA genome of about 12 kb, which codes for two polyproteins that give rise to non-structural and structural proteins, including the capsid. Moreover, upon viral replication, a long dsRNA intermediate, which can be sensed by the host antiviral machinery, accumulates. Of note, SINV dsRNA can be cleaved into siRNA in insects as well as in human cells expressing the Drosophila DICER-2 protein (Girardi et al., 2015). Nonetheless, although human DICER has the potential to interact with the viral RNA duplex, we did not find evidence that SINV dsRNA could be processed into siRNAs in somatic mammalian cells (Girardi et al., 2013, 2015). We thus hypothesized that specific proteins could interfere with DICER during SINV infection by direct interaction and limit its accessibility and/or activity. To address this hypothesis, we generated HEK293T cells expressing a tagged version of human DICER that could be immunoprecipitated in mock or SINV-infected cells in order to perform a proteomic analysis of its interactome. Among the proteins co-immunoprecipitated with DICER and that were specifically enriched upon infection, we identified dsRBPs such as ADAR1, DHX9, PACT and PKR. We further validated the direct

interaction between DICER and PKR upon SINV infection. We also demonstrated that the interactions of the endogenous DICER with PKR, PACT and DHX9 could also be detected in SINV-infected, but not mock-infected, HCT116 cells. We dissected the protein domains necessary for this interaction and we found that DICER helicase domain plays a fundamental role as a recruitment platform for PKR but also for other co-factors. Finally, we also show that expression of a helicase-truncated version of DICER has a negative effect on SINV infection. Our results indicate that DICER interactome is highly dynamic and directly link components of RNAi and IFN pathways in modulating the cellular response to viral infection.

Results

Establishment of a HEK293T cell line expressing FLAG-HA tagged DICER

In order to be able to study the interactome of the human DICER protein during viral infection, we transduced *Dicer* knock-out HEK293T cells (NoDice 2.20) (Bogerd et al., 2014a) with either a lentiviral construct expressing a FLAG-HA-tagged wild type DICER protein (FHA:DICER WT #4) or a construct without insert as a negative control (FHA:ctrl #1). After monoclonal selection of stably transduced cells, we first characterized one clone of both FHA:DICER WT and of the FHA:ctrl cell lines. We first confirmed that the expression of the tagged version of DICER restored the miRNA biogenesis defect observed in the NoDice cells (Fig. S1A). We then monitored the phenotype of these cells during SINV infection by using as a readout of viral infection the modified version of SINV able to express GFP from a duplicated sub-genomic promoter (SINV-GFP) (López et al, 2020). At 24 hours post-infection (hpi) and a multiplicity of infection (MOI) of 0.02, the GFP fluorescence observed in FHA:DICER WT #4 cells and HEK293T cells was similar. However, the NoDice FHA:ctrl #1 cells displayed a decrease in GFP signal (Fig. 1A). Western blot analysis of GFP expression confirmed the observations by epifluorescence microscopy, *i.e.* a significantly lower accumulation of GFP in

the absence of the DICER protein (Fig. 1B). We therefore wished to confirm the effect of DICER loss on SINV-GFP infection in another NoDice cell line, *i.e.* the NoDice clone 4.25 (Bogerd et al., 2014b), and in another clone of the NoDice 2.20 FHA:ctrl cells (NoDice FHA:ctrl #2). We observed a similar decrease of SINV-GFP infection in NoDice 2.20 cells and two independent NoDice FHA:ctrl clones compared to HEK293T cells as shown by GFP microscopy (Fig. S1B), by titration of the virus (Fig. S1C) and by western blot analysis (Fig. S1D). However, the independent NoDice 4.25 *Dicer* knock-out clone appeared mostly unaffected compared to HEK293T cells in term of GFP accumulation and viral titer (Fig. S1B-D). This suggests that, despite the observed slight effect on SINV-GFP in NoDice 2.20 cells (Fig. 1), DICER antiviral effect is not reproductible in an independent clone and therefore could not be generalized.

In order to evaluate whether different expression levels of DICER in a NoDice background could rescue the SINV infection phenotype observed in HEK293T cells, we also infected both the FHA:DICER WT polyclonal and an independent FHA:DICER WT clone (FHA:DICER WT #17) with SINV-GFP (Fig. 1A and Fig. 1C-D). We confirmed that the GFP fluorescence observed by microscopy (Fig. 1A), as well as the viral titers and the GFP protein accumulation (Fig. 1C-D) in all tested FHA:DICER lines were comparable to the ones observed in HEK293T cells. Moreover, there was no striking differences in AGO2 expression between the FHA:DICER lines (Fig. 1D).

Altogether, these results indicate that the FHA-tagged DICER protein can functionally complement the lack of DICER in terms of miRNA biogenesis (Fig. S1A) and can therefore be used for proteomics studies. Moreover, because we could not observe significant differences in terms of SINV infection (Fig. 1) between the different FHA:DICER clones tested, we decided to select one line, namely FHA:DICER WT#4, for further analysis.

158 **Analysis of DICER interactome during SINV infection by mass spectrometry**

159 Our molecular tool being validated, we then focused on determining the interactome of
160 FHA:DICER during SINV infection. We wanted to look at DICER interactome at an early
161 infection time point to isolate cellular factors that could potentially modulate either DICER
162 accessibility or its effect on viral dsRNA. As SINV replicates quickly upon cellular entry, we
163 chose to set up the infection conditions to a duration of 6 hours at an MOI of 2.

164 We performed an anti-HA immunoprecipitation experiment (HA IP) coupled to label-
165 free LC-MS/MS analysis in FHA:DICER WT #4 cells either mock-infected or infected for 6 h
166 at an MOI of 2 with SINV-GFP. In parallel, we performed an anti-MYC immunoprecipitation
167 as a negative control (CTL IP). The experiments were performed in technical triplicate in order
168 to have statistically reproducible data for the differential analysis, which was performed using
169 spectral counts. Prior to the detailed analysis of the results, we verified that there was no
170 confounding factor in the experimentation by performing a Principal Component Analysis
171 (PCA). This allowed us to see that the replicates were very homogenous and that the different
172 samples were well separated based on the conditions.

173 To check the specificity of the HA immunoprecipitation, we first compared the proteins
174 identified in the HA IP with the ones identified in the CTL IP in mock-infected cells.
175 Differential expression analysis allowed us to calculate a fold change and an adjusted p-value
176 for each protein identified and to generate a volcano plot representing the differences between
177 HA and CTL IP samples. Applying a fold change threshold of 2 ((LogFC) > 1), an adjusted p-
178 value threshold of 0.05 and a cutoff of at least 5 spectral counts in the most abundant condition,
179 we identified 258 proteins differentially immunoprecipitated between the two conditions out of
180 1318 proteins (Fig. 2A and Supp. Table 1). Among these, 123 proteins were specifically
181 enriched in the HA IP. The most enriched protein was DICER, followed by its known co-factors
182 TRBP and PACT (also known as PRKRA) (Chendrimada et al., 2005; Lee et al., 2006). We

were also able to retrieve AGO2, indicating that the RISC loading complex was immunoprecipitated and that proteins retrieved in our HA IP are specific to DICER immunoprecipitation.

We next performed the differential expression analysis of proteins retrieved in the HA IP in SINV-GFP compared to mock-infected cells. Among 1342 proteins, 296 were differentially retrieved between conditions (Fig. 2B and Supp. Table 2). Of these, 184 proteins, including viral ones, were at least 2-fold enriched in SINV-GFP-infected cells. GO-term analysis showed a significant enrichment in RNA binding proteins including double-stranded RNA binding proteins and RNA helicases (Fig. 2C). Among the RNA binding proteins retrieved, the top and most specific DICER interactor is the interferon-induced, double-stranded (ds) RNA-activated protein kinase PKR (also known as E2AK2), which is enriched more than 250 times in virus-infected cells (Fig. 2B and D). We were also able to identify the dsRNA-specific adenosine deaminase protein ADAR-1 (also known as DSRAD), as well as PACT, which were enriched 5.9 and 4.2 times respectively in SINV-GFP-infected cells compared to mock-infected cells (Fig. 2B and D). Among the isolated RNA helicases, we identified the ATP-dependent RNA helicase A protein DHX9, which is implicated in *Alu* element-derived dsRNA regulation and in RISC loading (Aktaş et al., 2017; Robb and Rana, 2007). In order to verify if the observed interactions were specific to SINV we performed the same experiments with another virus of the *Togaviridae* family, the Semliki forest virus (SFV). In this analysis, we were able to retrieve ADAR-1, DHX9, PACT and PKR, specifically enriched in SFV-infected samples (Fig. S2 and Supp. Tables 3 and 4). These results show that these interactions can be retrieved in *Togaviridae*-infected cells.

Taken together, our data indicate that several proteins interacting with DICER in virus-infected cells are involved in dsRNA sensing and/or interferon-induced antiviral response.

DICER and PKR interact *in vivo* in the cytoplasm during SINV infection

To validate the LC-MS/MS analysis, we performed a co-immunoprecipitation (co-IP) followed by western blot analysis in FHA:DICER WT #4 cells infected with SINV-GFP at an MOI of 2 for 6 h. Whereas TRBP interacted equally well with FHA:DICER in mock and SINV-GFP-infected cells, ADAR-1, PKR, DHX9 and PACT were only retrieved in the HA IP in SINV-infected cells (Fig. 3A). We verified that these interactions could also be observed at a later time post-infection by performing the HA IP in FHA:DICER WT #4 cells infected with SINV-GFP for 24 h at an MOI of 0.02. This indicates that the specific interactions between DICER and ADAR-1, DHX9, PACT or PKR occur at an early stage of the SINV infection and remain stable in time in virus-infected cells (Fig. S3A).

In order to verify whether these interactions were mediated by RNA, we performed an anti-HA co-IP experiment on an RNase A/T1 treated total extract from FHA:DICER WT #4 cells infected with SINV-GFP at an MOI of 2 for 6h. We confirmed the efficiency of the RNase treatment by ethidium bromide staining visualisation of total RNA on an agarose gel (Fig. S3B). TRBP equally interacted with FHA:DICER, with or without RNase treatment, in mock and SINV-GFP-infected cells (Fig. 3B). Instead, the virus-induced interactions between DICER and PKR or PACT upon SINV-GFP infection were almost totally lost in the RNase-treated samples. Upon virus infection, PKR is phosphorylated to be activated and exert its antiviral function (Lemaire et al., 2008). Using an antibody targeting the phosphorylated form of PKR (p-PKR), we looked for p-PKR before and after RNase treatment. The virus-enriched interactions between DICER and p-PKR or DHX9 were completely lost upon RNase treatment. These results therefore indicate that RNA molecules (either single- or double-stranded) facilitate DICER interaction with DHX9, PACT and PKR and its active form, although the complex may also partially interact in an RNA-independent manner.

Because of the involvement of PKR in antiviral response (García et al., 2007) and the fact that it shares common co-factors with DICER, namely TRBP and PACT (Haase et al., 2005; Patel et al., 2000), we decided to focus our analysis on the DICER-PKR interaction. To confirm the biological relevance of this interaction, we first performed a reverse co-IP to immunoprecipitate the endogenous PKR protein in HEK293T cells infected or not with SINV-GFP. While PACT interacted with PKR both in mock and in SINV-GFP-infected cells as expected (Fig. 3C lower panel), DICER co-immunoprecipitated with the endogenous PKR only in virus-infected cells as previously observed (Fig. 3C upper panel).

To further determine whether DICER and PKR could directly interact *in vivo*, we set up a bi-molecular fluorescent complementation assay (BiFC) experiment (Lepur et al., 2016). To this end, we fused the N- or C-terminal halves of the Venus protein ($^{N\text{-ter}}$Venus or $^{C\text{-ter}}$Venus) to DICER and to PKR but also to TRBP and PACT. Since we showed above that an N-terminally tagged DICER was functional, we fused the Venus fragments at the N-terminal end of DICER. For the other three proteins, we fused the Venus fragments at the N- or C-terminus and selected the best combination. To avoid interaction with the endogenous DICER and PKR proteins, we conducted all BiFC experiments in NoDice/ΔPKR HEK293T cells (Kennedy et al., 2015). In order to control the BiFC experiments, we chose to exploit the well characterized DICER-TRBP interaction, which is known to occur via the DICER DEAD-box helicase domain (Daniels et al., 2009). We therefore used the wild-type DICER protein as a positive control and a truncated version of DICER protein lacking part of this helicase domain and called DICER N1 (Kennedy et al., 2015) as a negative control (Fig. S3C). We first confirmed the expression of the tagged proteins by western blot analysis (Fig. S3D) and then, we tested the interactions between DICER and TRBP or PACT or PKR. We co-transfected the Venus constructs for 24 h and then infected cells with SINV or not for 6 h at a MOI of 2. A comparable fluorescent signal was observed both in mock- and SINV-infected cells when $^{N\text{-ter}}$Venus:DICER was co-

transfected with either PACT or TRBP fusion construct (Fig. 3D). Although we initially expected an increase of the Venus fluorescence in SINV-infected cells, overall we observed a similar signal for the DICER-PKR interaction both in mock- and SINV-infected cells, probably due to the fact that both proteins are transiently overexpressed in this experiment.

As a control and to rule out any aspecific interactions between the different proteins tested, we also monitored the DICER-N1-TRBP interaction by BiFC. As expected, no fluorescent signal was observed in cells co-transfected with $^{N\text{-ter}}$Venus:DICER N1 and TRBP:Venus$^{C\text{-ter}}$ (Fig. S3E), confirming that DICER helicase domain is required for its interaction with TRBP (Daniels et al., 2009) and validating the specificity of the BiFC approach.

To further confirm that the absence of PKR did not influence the interactions of TRBP or PACT with DICER, we also performed a BiFC analysis in HEK293T cells. After verifying that in this context as well, fusion proteins were expressed as expected (Fig. S3F), we observed that the results were similar as in NoDiceΔPKR cells (Fig. S3G).

To gain more insight into the subcellular localization of these interactions during SINV infection, we performed the BiFC experiments, fixed the cells and observed them under a confocal microscope. We observed a cytoplasmic fluorescent signal for DICER-TRBP and DICER-PACT interactions (Fig. 3E upper and middle panels), which is in agreement with their canonical localization for the maturation of most miRNAs (Bernstein et al., 2001; Hutvágner et al., 2001). Similarly, co-transfection of DICER and PKR led to a strong Venus signal homogeneously distributed in the cytoplasm (Fig. 3E lower panel).

Collectively, these results formally confirm that DICER interacts with several RNA helicases and dsRNA-binding proteins in virus-infected cells, among which PKR, and that for the latter this interaction occurs in the cytoplasm.

DICER interactome changes upon SINV infection are not cell-type specific

To further validate our previous DICER interactome results and generalize them to another biological system, we performed co-IP experiments on the endogenous DICER in a different cell type. To this end, the FLAG-HA-GFP tag was knocked into (KI) the *Dicer* locus in human colon carcinoma cells (HCT116) by CRISPR-Cas9-mediated homologous recombination (Fig. S4A-C). A guide RNA (gRNA) targeting the region corresponding to Dicer ATG and a DNA template for homologous recombination bearing the FLAG-HA-GFP sequence surrounded by the upstream and downstream arms of Dicer were used to generate the resulting cell line referred to as HCT116 KI-DICER cells. The expected insertion of the tag in one of the two Dicer allele was assessed by PCR amplification and Sanger sequencing (Fig. S4A-C). In agreement, we could detect two bands for DICER protein by western blot in the HCT116 KI-DICER cells, which confirmed that this cell line is heterozygous (Fig. 4A).

We additionally verified the expression of specific DICER-interacting proteins, such as AGO2, PKR or TRBP, in HCT116 KI-DICER cells compared to the parental HCT116 cells and to HEK293T cells (Fig. 4A). We also measured the production of mature miRNAs, such as miR-16, by northern blot analysis and confirmed that miRNA expression is maintained in HCT116 KI-DICER cells (Fig. 4B). Of note, the GFP inserted at the *Dicer* locus could not be detected by epifluorescence microscopy in the HCT116 KI-DICER cells, which probably reflects the low abundance of the DICER protein.

We then determined whether SINV-GFP infection was comparable in HCT116 cells and HEK293T cells. We infected HCT116, HCT116 KI-DICER and HEK293T cells with SINV-GFP at three different MOI (0.02, 0.1 and 1) and measured GFP fluorescence by microscopy at 24 hpi (Fig. 4C). Both HCT116 and HCT116 KI-DICER cells expressed GFP upon infection with SINV-GFP, although with a lower intensity than HEK293T cells. We also verified by western blot analysis the accumulation of GFP and the phosphorylation of both PKR and eIF2α

upon SINV-GFP infection of HCT116 KI-DICER and HEK293T cells (Fig. S4D) and chose as optimal SINV-GFP condition of infection in HCT116 KI-DICER cells the MOI of 0.1 for 24h.

To validate the DICER interactions observed in HEK293T FHA:DICER cells, we then performed anti-HA co-IP experiments followed by western blot analysis in HCT116 KI-DICER cells infected or not with SINV-GFP. We successfully retrieved TRBP interacting with DICER in both mock and infected cells, whereas DHX9, PKR (phosphorylated or not) and PACT were only retrieved in the HA IP in infected cells (Fig. 4D). These results not only confirm that the endogenous DICER specifically interacts with DHX9, PACT and PKR upon SINV infection, but also that these interactions are not restricted to one specific cell type.

The helicase domain of DICER is required for its interaction with PKR

Even though DICER and PKR are likely brought together by RNA, specific protein domains might be involved in stabilizing the complex. We therefore next determined the domain of DICER required for its interaction with PKR. Since its helicase domain was previously shown to be involved in the interaction with TRBP and PACT (Daniels et al., 2009; Lee et al., 2006), we speculated that it could also be implicated in binding PKR. To test this hypothesis, we cloned several versions of DICER proteins wholly or partly deleted of the helicase domain (Fig. 5A DICER N1 and N3). In addition, we also cloned the helicase domain alone (Fig. 5A DICER Hel.) and a DICER variant deleted of its C-terminal dsRNA binding domain (Fig. 5A DICER ΔdsRBD) since this domain could also be involved in protein-protein interaction (Doyle et al., 2013; Lambert et al., 2016). We then transfected the different versions of DICER WT and the deletion mutant constructs in NoDice cells. In mock and SINV-GFP infected cells, whole cell extracts were subjected to anti-HA and anti-MYC (CTL) IP. TRBP was retrieved in both conditions with DICER WT, Hel. and ΔdsRBD (Fig. 5B and 5C). In mock cells, PACT and PKR were only found weakly interacting with DICER WT (Fig. 5B). In SINV-infected cells,

we observed that similar to TRBP and to a lesser extent PACT, N1 and N3 mutations strongly reduced the binding of DICER with PKR (Fig. 5C lanes 2-3 and 7-8). Importantly, we also noted that the helicase domain alone could bind PKR, TRBP and PACT (Fig. 5C lanes 4 and 9). Moreover, the deletion of the dsRNA binding domain of DICER did not affect its interaction with TRBP, PACT and PKR (Fig. 5C lanes 5 and 10). We also looked for p-PKR in our co-IP (Fig. 5C panel p-PKR). We noticed that only WT DICER and its helicase domain were able to interact with p-PKR (Fig. 5C lanes 1&6 and 4&9). The fact that DICER ΔdsRBD did not interact with p-PKR (Fig. 5C lanes 5&10) is striking but could indicate that the phosphorylation of PKR may induce conformation changes preventing its interaction with some domains of DICER. These results reveal that, like for TRBP and PACT, the helicase domain of DICER is required for DICER-PKR/p-PKR interaction during SINV infection.

In order to confirm these co-IP experiments, we next decided to perform BiFC experiments using the same conditions as previously. In both mock and SINV-infected cells, only the combinations of DICER WT-PKR and DICER ΔdsRBD-PKR showed a strong Venus signal, while neither DICER N1 nor N3 constructs revealed an interaction with PKR (Fig. 5D). In contrast, the DICER Hel. construct did not seem to interact with PKR in mock-infected cells but appeared to do so in SINV-infected cells as a faint Venus signal could be observed. These results therefore confirmed the co-IP observations for the DICER-PKR interaction. In addition, we also performed a BiFC experiment using the different DICER constructs with TRBP or PACT. Altogether, the BiFC results mostly fitted with the co-IP experiment for the DICER-TRBP (Fig. S5A) and DICER-PACT (Fig. S5B) interactions. TRBP indeed did not seem to interact with the DICER N1 and only slightly with the DICER N3. However, PACT interaction was lost with DICER N1, but not with DICER N3 in mock- and SINV-infected cells (Fig. S5B third panel). This result may be explained by the fact that DICER interacts with PACT *via* the helicase and DUF domains, whereas only the DICER helicase domain is required for its

357 interaction with TRBP (Daniels et al., 2009; Lee et al., 2006). In agreement, the Venus signal
358 observed between the DICER Hel. and PACT seemed weaker than the one we observed with
359 TRBP (Fig. S5A and B fourth panels).
360 Taken together these results indicate that DICER interacts with both PKR and its
361 phosphorylated form during SINV infection and that this interaction requires the helicase
362 domain of DICER.
363
364 **Functional importance of DICER helicase domain during SINV infection**
365 We finally sought to study the functional role of DICER-PKR interaction during viral infection.
366 For this purpose, we decided to use DICER helicase deletion mutants to study SINV infection.
367 To do so, we first generated NoDice HEK293T cells stably expressing FHA-tagged DICER N1
368 (FHA:DICER N1) by lentiviral transduction. As for the FHA:DICER WT cell line, we first
369 selected a clone expressing the tagged DICER N1 at a level similar level to the endogenous
370 DICER protein in HEK293T cells (Fig. 6A). DICER N1 protein has been shown to still be able
371 to produce miRNAs (Kennedy et al., 2015). We thus verified by northern blot analysis that
372 DICER N1 is indeed able to process miRNAs similarly to WT DICER in HEK 293T and
373 FHA:DICER cells, thereby validating the functionality of the tagged protein (Fig. 6B). We next
374 infected HEK293T, FHA:DICER WT #4 and FHA:DICER N1 #6 cells with SINV-GFP and
375 measured virus accumulation by assessing GFP expression by microscopy analysis.
376 Interestingly, the GFP protein level was drastically reduced in FHA:DICER N1 #6 cells
377 compared to FHA:DICER WT #4 and HEK293T cells (Fig. 6C). Encouraged by this
378 observation, we decided to infect with SINV-GFP additional DICER deletion mutants, namely
379 N3 and Hel. We generated stable cell lines for these various mutants by lentiviral transduction
380 in the NoDice 2.20 background and infected those cells with SINV-GFP at an MOI of 0.02 for
381 24h. We verified by western blot analysis that all selected DICER mutant clones, namely N1

#6, N3 #2.13 and Hel. #2.6, expressed the tagged protein at the expected size and at levels mostly similar to the FHA:DICER WT #4 line (Fig. 6D, first two panels). We also verified the DICER mutants contribution to the endogenous miRNA biogenesis by performing a northern blot analysis on miR-16 accumulation (Fig. S6A).

We additionally verified the impact of these DICER mutants on SINV-GFP infection by measuring the GFP intensity of fluorescence by microscopy (Fig. S6B). Our results indicated that GFP accumulation is similar in HEK293T, NoDice 2.20, FHA:DICER WT, Hel. and ctrl cells. However, almost no fluorescence was detected in FHA:DICER N1 #6 and N3 #2.13 cells compared to HEK293T cells (Fig. S6B). The reduction of virus-encoded GFP accumulation and viral production were confirmed by western blot (Fig. 6D) and by plaque assay, respectively (Fig. 6E).

Altogether, these results therefore indicate that expressing a helicase truncated version of DICER, which is unable to interact with PKR, appears to confer an antiviral phenotype to SINV infection.

Discussion

The role of DICER in antiviral defense in human cells remains a topic of intense discussion (Cullen et al., 2013; Maillard et al., 2013, 2019; Cullen, 2017). In particular there have been contradictory reports regarding its capacity to produce siRNAs from viral RNAs (Bogerd et al., 2014a; Parameswaran et al., 2010; Donaszi-Ivanov et al., 2013; Backes et al., 2014). These observations could be due to the fact that several mammalian viruses potentially encode VSR proteins, thereby masking the effect of RNAi (Li et al., 2013, 2016; Maillard et al., 2013; Qiu et al., 2017, 2020). Another putative but non-exclusive explanation could be that there is a mutual regulation of type I IFN and RNAi pathways (Berkhout, 2018; Takahashi and Ui-Tei, 2020). Thus, it has already been shown that PACT can regulate MDA5 and RIG-I during virus

407 infection and therefore the induction of type I IFN response (Kok et al., 2011; Lui et al., 2017).
408 To date, it is not clear whether the activity of the DICER protein as well could be regulated by
409 potential interactors, or inversely whether it could itself modulate the activity of proteins
410 involved in the IFN pathway. To answer this question, we determined the changes in the
411 interactome of human DICER upon SINV and SFV infection. This analysis allowed us to reveal
412 that a lot of proteins associating with DICER during viral infection are dsRNA-binding proteins
413 and RNA helicases. A number of these proteins are known to be involved in antiviral defense
414 pathways, thereby indicating the possible formation of one or several complexes between
415 DICER and these proteins, which are very likely brought together by the accumulation of
416 dsRNA during virus infection.

417 Among these proteins, we chose to focus on the well-known ISG PKR, which is
418 involved in many cellular pathways such as apoptosis, cellular differentiation, development and
419 antiviral defense (Clemens, 1997; Gal-Ben-Ari et al., 2018; Kim et al., 2014; Lemaire et al.,
420 2008). PKR is one of the main actors of the Integrative Stress Response (ISR) in human cells,
421 and its activation or inhibition needs to be tightly regulated in order to have a properly balanced
422 response to stress. Our results indicate that DICER interacts via its helicase domain with PKR
423 in the cytoplasm during SINV infection. The helicase domain of DICER, which is also required
424 for its interaction with TRBP and PACT, belongs to the helicase superfamily 2, which is also
425 found in RLRs such as RIG-I, MDA5 or LGP2 (Ahmad and Hur, 2015; Fairman-Williams et
426 al., 2010). These proteins act as sensors of viral infection and through the activation of proteins
427 such as MAVS, mediate the induction of type I IFN pathway (Ahmad and Hur, 2015). We
428 hypothesize that even though the human DICER helicase has evolved mainly to act in
429 miRNA/siRNA pathway, it still retained the capacity to act as an RLR. However, as opposed
430 to RIG-I and MDA5, our data suggest that DICER would act more as an inhibitor rather than

inducer of the immune response. Therefore, we propose that this domain serves as a platform for the recruitment of different proteins to diversify the function of DICER.

One such regulatory effect appears to be on the antiviral activity of PKR, as cells expressing a truncated form of DICER unable to interact with PKR become resistant to SINV infection. This is in agreement with previous observations that ectopic expression of the *Drosophila* DICER2 protein in human cells perturbs IFN signaling pathways and antagonizes PKR-mediated antiviral immunity (Girardi et al., 2015). The exact mechanism involved is still unclear and will require further work, but it seems that the two proteins are likely brought together *via* their interaction with RNA, most probably of viral origin. Indeed, we showed that the co-IP interaction was partially RNase sensitive. However, we confirmed that the interaction is not artificially created during the co-immunoprecipitation procedure, since we could show that DICER and PKR interact in BiFC assay, a technique that favors the detection of direct interactions (Lepur et al., 2016). Most of the time, the inhibition of PKR activity relies on its inhibition to bind to dsRNA or to auto-phosphorylate. For example, the human tRNA-dihydrouridine synthase 2 (hDus2) binds the first dsRBD of PKR and prevents its activation (Mittelstadt et al., 2008). TRBP binds dsRNAs but also PKR directly hindering its dimerization. In normal condition, TRBP is also associated with PACT thus preventing PKR activation by PACT (Park et al., 1994; Nakamura et al., 2015; Daher et al., 2009; Singh et al., 2011). Since we showed that DICER can bind the activated phospho-PKR, we hypothesize that this interaction does not result in the inhibition of PKR autophosphorylation. In fact, in condition of infection with a high virus dose, we showed that phospho-PKR levels are similar in cells expressing DICER WT or helicase deletion mutants N1 and N3, but the activated PKR does not associate with these truncated versions of DICER. Therefore, one possibility could be that DICER interaction with PKR prevents the latter from acting upon some of its targets, which remain to be identified, to fine-tune the antiviral response.

As of now, we cannot formally rule out that the effect of DICER on PKR is mediated by other proteins. TRBP and PACT have been shown to regulate PKR activity, the former normally acting as a repressor and the latter as an activator (Nakamura et al., 2015; Patel et al., 2000; Singh et al., 2011). Interestingly, in lymphocytic Jurkat cells infected by HIV-1, PACT can also act as a repressor of PKR (Clerzius et al., 2013). It is thus tempting to speculate that these two proteins participate in the formation of the DICER-PKR complex. However, our results show that this may not necessarily be the case. Indeed, in the BiFC experiment, the DICER N3 mutant still interacted with PACT but not with PKR indicating that PACT binding is not sufficient to confer the association with PKR.

Besides PKR, other proteins were specifically enriched upon viral infection in the DICER IP. These are also interesting candidates to explain the putative regulatory role of DICER. Among these proteins, DHX9 and ADAR-1 are especially intriguing. DHX9, also known as RNA helicase A (RHA), associates with RISC, helping the RISC loading (Robb and Rana, 2007). Moreover, DHX9 is directly involved in removing toxic dsRNAs from the cell to prevent their processing by DICER (Aktaş et al., 2017). It has also been implicated in HIV-1 replication and knockdown of DXH9 leads to the production of less infectious HIV-1 virions (Li et al., 1999; Fujii et al., 2001; Roy et al., 2006). Finally, DXH9 interacts with and is phosphorylated by PKR in mouse embryonic fibroblasts. This phosphorylation precludes the association of DHX9 with RNA, thus inhibiting its proviral effect (Sadler et al., 2009). In light of these observations and ours, we can speculate that the inhibitory effect of DICER on PKR activity could also be linked to DHX9 phosphorylation. ADAR-1 is one of the well-known RNA-editing factors (Herbert et al., 1997). ADAR-1 is linked to both miRNA biogenesis (Iizasa et al., 2010; Ota et al., 2013; Yang et al., 2006) and virus infection. Indeed, ADAR-1 has an antiviral effect against Influenza virus, but most of the time, its depletion leads to a decrease of the viral titer, as was reported for VSV or HIV-1 (Li et al., 2010; Samuel, 2011). It has been

481 shown that ADAR-1 and PKR interact directly during HIV-1 infection. This interaction triggers
482 the inhibition of PKR activation, and thus a reduction of eIF2α phosphorylation leading to an
483 increase of virus replication (Pfaller et al., 2011; Clerzius et al., 2009). Interestingly, over-
484 expression of ADAR-1 enhances drastically the replication of the alphaviruses Chikungunya
485 virus (CHIKV), and Venezuelan equine encephalitis virus (VEEV) most likely by interfering
486 with the IFN induction (Schoggins et al., 2011).

487 Finally, we cannot formally rule out that the virus resistance phenotype of the DICER
488 N1 and N3 cell lines is due to an increased processivity of these truncated proteins on long
489 dsRNA substrates (Kennedy et al., 2015), which would render DICER RNAi proficient.
490 However, PKR is still expressed in these cells, and is therefore expected to be predominant over
491 DICER for viral dsRNA sensing. It is nonetheless possible that its interaction with several
492 dsRNA binding proteins could also participate in limiting the efficiency of the helicase domain
493 of DICER, on top of its intrinsic lack of processivity (Chakravarthy et al., 2010).

494 Deciphering the exact role of human DICER protein during virus infection is a
495 challenging task and additional studies will be required to get a global picture. Nevertheless, by
496 assessing the interactome of this protein during SINV infection, we have unveiled a new role
497 for the helicase domain of DICER in regulating the cellular response to viral infection.

498

499 ## Material and methods

500 ### Plasmids, cloning and mutagenesis

501 Plasmids used for BiFC experiments were a gift from Dr. Oliver Vugrek from the Ruđer
502 Bošković Institute and described in (Lepur et al., 2016). The cDNAs of TRBP, PACT and PKR
503 were respectively amplified from (pcDNA-TRBP Addgene #15666) (Kok et al., 2007),
504 (pcDNA-PACT Addgene #15667) (Kok et al., 2007), (pSB819-PKR-hum Addgene #20030)
505 (Elde et al., 2009), and cloned into the four pBiFC vectors by Gateway recombination. DICER

N1, N3 Hel. and ΔdsRBD were generated by PCR mutagenesis from pDONR-DICER described in (Girardi et al., 2015) and cloned into the four pBiFC and pDEST-FHA vectors by Gateway recombination. plenti6 FHA-V5 vector was modified from plenti6-V5 gateway vector (Thermo Fisher scientific V49610) by Gibson cloning. DICER WT, N1 from pDONOR plasmids were cloned into plenti6 FHA-V5 by Gateway recombination. All primers used are listed in Supp. Table 5.

Cell lines

HEK293T, HEK293T/NoDice (2.20 and 4.25), and HEK293T/NoDiceΔPKR cell lines were a gift from Pr. Bryan Cullen and described in (Bogerd et al., 2014b; Kennedy et al., 2015). HCT116 cell line was a gift from Dr. Christian Gaiddon.

Generation of Flag-HA-GFP-DICER knock-in cell line by CRISPR/Cas9

To generate the knock-in cell line, the sequence of Flag-HA-GFP was amplified by PCR from the Flag-HA-GFP plasmid (Meister et al., 2005). DNA sequences corresponding to 1 Kb upstream (left homology arm) and downstream (right homology arm) the starting codon (ATG) of DICER gene were amplified from HCT116 cell genomic DNA using primer pairs listed in Supp. Table 5. The three PCR products were gel-purified and cloned into a linearized pUC19 by In-fusion cloning (Clontech) to obtain the template for homologous recombination (LarmDICER-FlagHAGFP-RarmDICER).

Design of the guide RNA targeting the region between Dicer 5'-UTR and its first coding exon for CRISPR/Cas9 mediated knock-in was carried out using the CRISPOR Design Tool (Concordet and Haeussler, 2018). Annealed oligonucleotide corresponding to the gRNA (Supp.

Table 5) were cloned into the vector pX459 (Addgene #48139) which also encodes *S. pyogenes* Cas9 with 2A-Puro.

The sequence of the donor plasmid was additionally mutagenized to disrupt the PAM sequence of the right homology arm to avoid its cleavage by the gRNA.

To obtain the knock-in (KI) cell line, 5 x 10^5 HCT116 cells were seeded in a 6 well plate with Dulbecco's modified Eagle medium (DMEM, Gibco®, Life Technologies) supplemented with 10% fetal bovine serum (FBS, Clontech) in a humidified atmosphere of 5% CO_2 at 37°C and transfected after 24 hours with the pX459-gRNADicerNterm-Cas9-2A-Puro plasmid and the Leftarm-FlagHAGFP-RightarmDICER donor plasmids at the ratio of 1 to 1 (6 micrograms plasmids in total) using Lipofectamine 2000 according to the manufacturer instructions. 24 hours later, puromycin (1mg/mL) was added to the cells to increase the KI efficiency and genomic DNA was isolated from individual colonies few days later.

The presence of the Flag-HA-GFP tag in frame with hDICER coding sequence was confirmed by sequencing PCR amplicon from KI cell gDNA. Expression of Flag-HA-GFP N-terminal tagged Dicer protein in the KI cells was confirmed by western blot.

Cell culture and transfection

Cells were maintained in Dulbecco's modified Eagle medium (DMEM, Gibco®, Life Technologies) supplemented with 10% fetal bovine serum (FBS, Clontech) in a humidified atmosphere of 5% CO_2 at 37°C. Transfection was performed using Lipofectamine 2000 (Invitrogen, ThermoFisher Scientific) according to the manufacturer's instructions.

Lentivirus production and generation of stable cell lines

The lentiviral supernatant from single transfer vector was produced by transfecting HEK293T cells (ATCC® CRL-3216™) with 20 µg of the transfer vector, 15 µg of pMDLg/p RRE and 10

554 µg of pRSV-Rev packaging plasmids (Addgene #12251 and Addgene #12253) and the pVSV
555 envelope plasmid (Addgene #8454) using Lipofectamine 2000 (Invitrogen, ThermoFisher
556 Scientific) reagent according to the manufacturer's protocol. Standard DMEM (Gibco®, Life
557 Technologies) medium supplemented with 10% Fetal bovine serum (FBS, Gibco®, Life
558 Technologies) and 100 U/mL of penicillin-Streptomycin (Gibco®, Life Technologies) was
559 used for growing HEK293T cells and for lentivirus production. One 10 cm plate of HEK293T
560 cells at 70-80% confluency was used for the transfection. The medium was replaced 8 hours
561 post-transfection. After 48 hours the medium containing viral particles was collected and
562 filtered through a 0.45μm PES filter. The supernatant was directly used for transfection or
563 stored at -80°C. A 6 well plate of HEK293T/NoDice cells at 80% confluency was transduced
564 using 600 μL of lentiviral supernatant either expressing FHADICER, N1 or empty vector,
565 supplemented with 4 ug/mL polybrene (Sigma) for 6 hours. The transduction media was then
566 changed with fresh DMEM for 24 hours and the resistant cell clones were selected for about 6
567 weeks with blasticidin (15 µg/mL) and subsequently maintained under blasticidin selection.
568
569 **Viral stocks, virus infection**
570 Viral stocks of SINV or SINV-GFP were produced as described in (Girardi et al., 2015). Cells
571 were infected with SINV or SINV-GFP at an MOI of 0.02, 0.1, 1 or 2 and samples were
572 collected at different time points as indicated in the figure legends.
573
574 **Analysis of viral titer by plaque assay**
575 Vero R cells were seeded in 96-well plates format and were infected with 10-fold serial
576 dilutions infection supernatants for 1 hour. Afterwards, the inoculum was removed, and cells
577 were cultured in 2.5% carboxymethyl cellulose for 72 hours at 37°C in a humidified atmosphere

of 5% CO_2. Plaques were counted manually under the microscope and viral titer was calculated according to the formula: *PFU/mL = #plaques/ (Dilution*Volume of inoculum)*

Western blot analysis

Proteins were extracted from cells and homogenized in 350 µL of lysis buffer (50 mM Tris-HCl pH 7.5, 150 mM NaCl, 5 mM EDTA, 1% Triton X-100, 0.5% SDS and Protease Inhibitor Cocktail (complete Mini; Sigma Aldrich)). Proteins were quantified by the Bradford method and 20 to 30 µg of total protein extract were loaded on 4-20% Mini-PROTEAN® TGX™ Precast Gels (Bio-Rad). After transfer onto nitrocellulose membrane, equal loading was verified by Ponceau staining. For PVDF membrane, equal loading was verified by Coomassie staining after transfer and blotting. Membranes were blocked in 5% milk and probed with the following antibodies: anti-hDicer (1:500, F10 Santa Cruz sc-136979) and anti-hDicer (1:1000, A301-937A Bethyl), anti-TRBP (1:500, D-5 Santa Cruz sc-514124), anti-PKR (1:2500, Abcam ab32506), anti-PACT (1:500, Abcam, ab75749), anti-HA (1:10000, Sigma, H9658), anti-DHX9 (1:500, Abcam ab26271), anti-p-eIF2a (1:1000, Ser-52 Santa Cruz sc-601670), anti-hADAR-1 (1:500 Santa Cruz sc-271854) anti-p-PKR (1:1000 Abcam ab81303) anti-GFP (1:10000, Roche 11814460001) and anti-Tubulin (1:10000, Sigma T6557). Detection was performed using Chemiluminescent Substrate (Pierce, ThermoFisher Scientific) and visualized on a Fusion FX imaging system (Vilber).

RNA extraction and northern blot analysis

Total RNA was extracted using Tri-Reagent Solution (Fisher Scientific; MRC, Inc) according to the manufacturer's instructions. Northern blotting was performed on 10 µg of total RNA. RNA was resolved on a 12% urea-acrylamide gel, transferred onto Hybond-NX membrane (GE Healthcare). RNAs were then chemically cross-linked to the membrane during 90 min at 65°C

603 using 1-ethyl-3-[3-dimethylaminopropyl]carbodiimide hydrochloride (EDC) (Sigma Aldrich).
604 Membranes were prehybridized for 30 min in PerfectHyb™ plus (Sigma Aldrich) at 50°C.
605 Probes consisting of oligodeoxyribonucleotides (see Supplementary Table 2) were 5′-end
606 labeled using T4 polynucleotide kinase (ThermoFisher Scientific) with 25 µCi of [γ-32P]dATP.
607 The labeled probe was hybridized to the blot overnight at 50°C. The blot was then washed twice
608 at 50°C for 20 min (5× SSC/0.1% SDS), followed by an additional wash (1× SSC/0.1% SDS)
609 for 5 min. Northern blots were exposed to phosphorimager plates and scanned using a
610 Bioimager FLA-7000 (Fuji).
611
612 **Immunoprecipitation**
613 Immunoprecipitation experiments were carried out either on tagged proteins or on endogenous
614 proteins.
615 *Tagged proteins*: Cells were harvested, washed twice with ice-cold 1× PBS (Gibco®, Life
616 Technologies), and resuspended in 550 µL of lysis buffer (50 mM Tris-HCl pH 7.5, 140 mM
617 NaCl, 1.5 mM $MgCl_2$, 0.1% NP-40), supplemented with Complete-EDTA-free Protease
618 Inhibitor Cocktail (complete Mini; Sigma Aldrich). Cells were lysed by 30 min incubation on
619 ice and debris were removed by 15 min centrifugation at 2000 g and 4°C. An aliquot of the
620 cleared lysates (50 µL) was kept aside as protein Input. Samples were divided into equal parts
621 (250 µL each) and incubated with 15 µL of magnetic microparticles coated with monoclonal
622 HA or MYC antibodies (MACS purification system, Miltenyi Biotech) at 4°C for 1 hour under
623 rotation (10 rpm). Samples were passed through μ Columns (MACS purification system,
624 Miltenyi Biotech). The μ Columns were then washed 3 times with 200 µL of lysis buffer and 1
625 time with 100 µL of washing buffer (20 mM Tris-HCl pH 7.5). To elute the immunoprecipitated
626 proteins, 95°C pre-warmed 2x Western blot loading buffer (10% glycerol, 4% SDS, 62.5 mM

627 Tris-HCl pH 6.8, 5% (v/v) 2-β-mercaptoethanol, Bromophenol Blue) was passed through the
628 *μ* Columns. Proteins were analyzed by western blotting or by mass spectrometry.
629 *Endogenous proteins*: The day before immunoprecipitation, magnetic DynaBeads protein G
630 (Invitrogen, ThermoFisher Scientific) were prepared: briefly, 160 µL of magnetic DynaBeads
631 protein G (Invitrogen) were washed three times with lysis buffer (50 mM Tris-HCl pH 7.5, 150
632 mM NaCl, 5 mM EDTA, 1% Triton X-100, 0.5% SDS). The beads were then incubated with 4
633 µg of BSA for 1 h under agitation at room temperature. An aliquot of beads (40 µL) was kept
634 for preclearing step. The remaining beads were incubated either with 6 µg of PKR antibody or
635 control IgG overnight at 4°C under rotation.
636 For the IP: Cells were harvested, washed twice with ice-cold 1× PBS (Gibco®, Life
637 Technologies) and resuspended in 1 mL of lysis buffer (50 mM Tris-HCl pH 7.5, 150 mM
638 NaCl, 5 mM EDTA, 1% Triton X-100, 0.5% SDS) supplemented with Complete-EDTA-free
639 Protease Inhibitor Cocktail (complete Mini; Sigma Aldrich). Cells were lysed by three 15 s
640 sonication steps followed by 30 min incubation on ice and debris were removed by 15 min
641 centrifugation at 16000 g and 4°C. After centrifugation, an aliquot was kept aside as protein
642 Input. Samples were incubated with beads alone for preclearing step for 1 hour at 4°C on wheel.
643 Samples were then put on magnetic racks and the supernatant transferred on new tubes
644 containing either beads coupled to PKR antibody or to control IgG. Samples were incubated on
645 wheel for 3 hours at 4°C. After incubation, samples were put on magnetic racks and beads were
646 washed three times with lysis buffer. After removal of supernatant, beads were eluted with 2x
647 western blot loading buffer and incubated for 10 min at 95°C under agitation. Proteins were
648 analyzed by western blotting.
649
650 **RNase treatment followed by co-IP**

On tagged proteins: Cells were harvested, washed twice with ice-cold 1× PBS (Gibco®, Life Technologies), and resuspended in 550 µL of lysis buffer (50 mM Tris-HCl pH 7.5, 140 mM NaCl, 1.5 mM $MgCl_2$, 0.1% NP-40), supplemented with Complete-EDTA-free Protease Inhibitor Cocktail (complete Mini; Sigma Aldrich). Cells were lysed by 30 min incubation on ice and debris were removed by 15 min centrifugation at 2000 g and 4°C. Lysate was treated or not with RNase A/T1 mix (ThermoFisher Scientific) and place at 37°C 30min. An aliquot of the cleared lysates (25 µL) was kept aside as protein Input and another aliquot (25 µL) was kept to assess RNase treatment efficiency. Co-IP was led as previously described.

Total RNA was extracted using Tri-Reagent Solution (Fisher Scientific; MRC, Inc) according to the manufacturer's instructions. RNA integrity upon treatment was verified on an 1% agarose gel containing ethidium bromide 10 mg/mL (Invitrogen, ThermoFisher Scientific) and revealed under UV on Gel Doc™ EZ system (Bio-Rad).

BiFC assay

Experiments were carried out in two different ways. For non-fixed cells, NoDiceΔPKR or HEK293T cells were seeded at the density of 1.2 x 10^5 cells per well in a 24-well plate. After 16 hours, cells were transfected with equimolar quantities of each plasmid forming BiFC couples. After 24 hours, cells were infected with SINV at an MOI of 2 and pictures were taken 6 hours post-infection using ZOE fluorescent cell imager (Bio-Rad). Proteins were collected with lysis buffer (50 mM Tris-HCl pH 7.5, SDS 0.05%, Triton 1%, 5 mM EDTA, 150 mM NaCl) supplemented with Complete-EDTA-free Protease Inhibitor Cocktail (complete Mini; Sigma Aldrich), and subjected to western blot analysis. For fixed cells, NoDice/ΔPKR cells were seeded at the density of 8.10^4 cells per well in 8-well Millicell® EZ Slides (Merck Millipore), transfected and infected as described previously. At 6 hours post-infection, cells were fixed with 4% formaldehyde and 0.2% glutaraldehyde for 10 min. Cells were then washed

676 with 1× PBS (Gibco®, Life Technologies) and stained with 10 μg/μL DAPI (Invitrogen,
677 ThermoFisher Scientific) in 1× PBS solution (Invitrogen, ThermoFisher Scientific) for 5 min.
678 Fixed cells were mounted on a glass slide with Fluoromount-G mounting media (Southern
679 Biotech). Images were acquired using confocal LSM780 (Zeiss) inverted microscope with an
680 argon laser (514x nm) and with ×40 immersion oil objective. All pictures obtained from BiFC
681 experiments were treated using FigureJ software (NIH).
682
683 **Mass spectrometry analysis**
684 Protein extracts were prepared for mass spectrometry as described in a previous study (Chicois
685 et al., 2018). Each sample was precipitated with 0.1 M ammonium acetate in 100% methanol,
686 and proteins were resuspended in 50 mM ammonium bicarbonate. After a reduction-alkylation
687 step (dithiothreitol 5 mM – iodoacetamide 10 mM), proteins were digested overnight with
688 sequencing-grade porcine trypsin (1:25, w/w, Promega, Fitchburg, MA, USA). The resulting
689 vacuum-dried peptides were resuspended in water containing 0.1% (v/v) formic acid (solvent
690 A). One sixth of the peptide mixtures were analyzed by nanoLC-MS/MS an Easy-nanoLC-1000
691 system coupled to a Q-Exactive Plus mass spectrometer (Thermo-Fisher Scientific, USA)
692 operating in positive mode. Five microliters of each sample were loaded on a C-18 precolumn
693 (75 µm ID × 20 mm nanoViper, 3 μm Acclaim PepMap; Thermo) coupled with the analytical
694 C18 analytical column (75 µm ID × 25 cm nanoViper, 3 μm Acclaim PepMap; Thermo).
695 Peptides were eluted with a 160 min gradient of 0.1% formic acid in acetonitrile at 300 nL/min.
696 The Q-Exactive Plus was operated in data-dependent acquisition mode (DDA) with Xcalibur
697 software (Thermo-Fisher Scientific). Survey MS scans were acquired at a resolution of 70K at
698 200 m/z (mass range 350-1250), with a maximum injection time of 20 ms and an automatic
699 gain control (AGC) set to 3e6. Up to 10 of the most intense multiply charged ions (≥2) were
700 selected for fragmentation with a maximum injection time of 100 ms, an AGC set at 1e5 and a

resolution of 17.5K. A dynamic exclusion time of 20 s was applied during the peak selection process.

Database search and mass-spectrometry data post-processing

Data were searched against a database containing Human and Viruses UniProtKB sequences with a decoy strategy (GFP, Human and Sindbis Virus SwissProt sequences as well as Semliki Forest Virus SwissProt and TrEMBL sequences (releases from January 2017, 40439 sequences)). Peptides were identified with Mascot algorithm (version 2.3, Matrix Science, London, UK) with the following search parameters: carbamidomethylation of cysteine was set as fixed modification; N-terminal protein acetylation, phosphorylation of serine / threonine / tyrosine and oxidation of methionine were set as variable modifications; tryptic specificity with up to three missed cleavages was used. The mass tolerances in MS and MS/MS were set to 10 ppm and 0.02 Da respectively, and the instrument configuration was specified as "ESI-Trap". The resulting .dat Mascot files were then imported into Proline v1.4 package (http://proline.profiproteomics.fr/) for post-processing. Proteins were validated with Mascot pretty rank equal to 1, 1% FDR on both peptide spectrum matches (PSM) and protein sets (based on score). The total number of MS/MS fragmentation spectra (Spectral count or SpC) was used for subsequent protein quantification in the different samples.

Exploratory and differential expression analysis of LC-MS/MS data

Mass spectrometry data obtained for each sample were stored in a local MongoDB database and subsequently analyzed through a Shiny Application built upon the R/Bioconductor packages msmsEDA (Gregori J, Sanchez A, Villanueva J (2014). msmsEDA: Exploratory Data Analysis of LC-MS/MS data by spectral counts. R/Bioconductor package version 1.22.0) and msmsTests (Gregori J, Sanchez A, Villanueva J (2013). msmsTests: LC-MS/MS Differential

Expression Tests. R/Bioconductor package version 1.22.0). Exploratory data analyses of LC-MS/MS data were thus conducted, and differential expression tests were performed using a negative binomial regression model. The p-values were adjusted with FDR control by the Benjamini-Hochberg method and the following criteria were used to define differentially expressed proteins: an adjusted p-value < 0.05, a minimum of 5 SpC in the most abundant condition, and a minimum fold change of 2 (abs(LogFC) > 1).

Data availability

The mass spectrometry proteomics data have been deposited to the ProteomeXchange Consortium via the PRIDE (Perez-Riverol et al., 2019) partner repository with the dataset identifier PXD019093 and 10.6019/PXD019093.

Acknowledgments

The authors would like to thank members of the Pfeffer laboratory for discussion, Pr. Bryan Cullen for the kind gift of the HEK293T NoDice and NoDice/ΔPKR cell lines and Dr. Oliver Vugrek for the BiFC plasmids.

This work was funded by the European Research Council (ERC-CoG-647455 RegulRNA) and was performed under the framework of the LABEX: ANR-10-LABX-0036_NETRNA and ANR-17-EURE-0023, which benefits from a funding from the state managed by the French National Research Agency as part of the Investments for the future program. This work has also received funding from the People Programme (Marie Curie Actions) of the European Union's Seventh Framework Program (FP7/2007-2013) under REA grant agreement n° PCOFUND-GA-2013-609102, through the PRESTIGE program coordinated by Campus France (to EG), and from the French Minister for Higher Education, Research and Innovation

(PhD contract to MB). The mass spectrometry instrumentation was funded by the University of Strasbourg, IdEx "Equipement mi-lourd" 2015.

Author contributions

SP and ML conceived the project. TCM, ML, EG and SP designed the work. TCM, MB, ML, EG and MM performed the experiments and analyzed the results. PH and JC performed the mass spectrometry analysis. BCWM designed software and analyzed the mass spectrometry results. SP coordinated the work and assured funding. TCM, MB and SP wrote the manuscript with input from the other authors. All authors reviewed and approved the final manuscript.

References

Adiliaghdam, F., Basavappa, M., Saunders, T.L., Harjanto, D., Prior, J.T., Cronkite, D.A., Papavasiliou, N., and Jeffrey, K.L. (2020). A Requirement for Argonaute 4 in Mammalian Antiviral Defense. Cell Rep. *30*, 1690-1701.e4.

Ahmad, S., and Hur, S. (2015). Helicases in Antiviral Immunity: Dual Properties as Sensors and Effectors. Trends Biochem. Sci. *40*, 576–585.

Aktaş, T., Avşar Ilık, İ., Maticzka, D., Bhardwaj, V., Pessoa Rodrigues, C., Mittler, G., Manke, T., Backofen, R., and Akhtar, A. (2017). DHX9 suppresses RNA processing defects originating from the Alu invasion of the human genome. Nature *544*, 115–119.

Backes, S., Langlois, R.A., Schmid, S., Varble, A., Shim, J.V., Sachs, D., and tenOever, B.R. (2014). The Mammalian Response to Virus Infection Is Independent of Small RNA Silencing. Cell Rep. *8*, 114–125.

Bartel, D.P. (2018). Metazoan MicroRNAs. Cell *173*, 20–51.

Berkhout, B. (2018). RNAi-mediated antiviral immunity in mammals. Curr. Opin. Virol. *32*, 9–14.

Bernstein, E., Caudy, A.A., Hammond, S.M., and Hannon, G.J. (2001). Role for a bidentate ribonuclease in the initiation step of RNA interference. Nature *409*, 363–366.

Bogerd, H.P., Skalsky, R.L., Kennedy, E.M., Furuse, Y., Whisnant, A.W., Flores, O., Schultz, K.L.W., Putnam, N., Barrows, N.J., Sherry, B., et al. (2014a). Replication of many human viruses is refractory to inhibition by endogenous cellular microRNAs. J. Virol. *88*, 8065–8076.

Bogerd, H.P., Whisnant, A.W., Kennedy, E.M., Flores, O., and Cullen, B.R. (2014b). Derivation and characterization of Dicer- and microRNA-deficient human cells. RNA *20*, 923–937.

Borden, E.C., Sen, G.C., Uze, G., Silverman, R.H., Ransohoff, R.M., Foster, G.R., and Stark, G.R. (2007). Interferons at age 50: past, current and future impact on biomedicine. Nat. Rev. Drug Discov. *6*, 975–990.

Chakravarthy, S., Sternberg, S.H., Kellenberger, C.A., and Doudna, J.A. (2010). Substrate-Specific Kinetics of Dicer-Catalyzed RNA Processing. J. Mol. Biol. *404*, 392–402.

Chen, E.Y., Tan, C.M., Kou, Y., Duan, Q., Wang, Z., Meirelles, G.V., Clark, N.R., and Ma'ayan, A. (2013). Enrichr: interactive and collaborative HTML5 gene list enrichment analysis tool. BMC Bioinformatics *14*, 128.

Chendrimada, T.P., Gregory, R.I., Kumaraswamy, E., Norman, J., Cooch, N., Nishikura, K., and Shiekhattar, R. (2005). TRBP recruits the Dicer complex to Ago2 for microRNA processing and gene silencing. Nature *436*, 740–744.

Chicois, C., Scheer, H., Garcia, S., Zuber, H., Mutterer, J., Chicher, J., Hammann, P., Gagliardi, D., and Garcia, D. (2018). The UPF1 interactome reveals interaction networks between RNA degradation and translation repression factors in Arabidopsis. Plant J. *96*, 119–132.

Clemens, M.J. (1997). PKR-a protein kinase regulated by double-stranded RNA. Int J Biochem Cell Biol *29*, 945–949.

Clerzius, G., Gélinas, J.-F., Daher, A., Bonnet, M., Meurs, E.F., and Gatignol, A. (2009). ADAR1 interacts with PKR during human immunodeficiency virus infection of lymphocytes and contributes to viral replication. J. Virol. *83*, 10119–10128.

Clerzius, G., Shaw, E., Daher, A., Burugu, S., Gélinas, J.-F., Ear, T., Sinck, L., Routy, J.-P., Mouland, A.J., Patel, R.C., et al. (2013). The PKR activator, PACT, becomes a PKR inhibitor during HIV-1 replication. Retrovirology *10*, 96.

Concordet, J.-P., and Haeussler, M. (2018). CRISPOR: intuitive guide selection for CRISPR/Cas9 genome editing experiments and screens. Nucleic Acids Res. *46*, W242–W245.

809 Cullen, B.R. (2006). Is RNA interference involved in intrinsic antiviral immunity in mammals?
810 Nat Immunol *7*, 563–567.
811 Cullen, B.R. (2017). RNA Interference in Mammals: The Virus Strikes Back. Immunity *46*,
812 970–972.
813 Cullen, B.R., Cherry, S., and tenOever, B.R. (2013). Is RNA Interference a Physiologically
814 Relevant Innate Antiviral Immune Response in Mammals? Cell Host Microbe *14*, 374–
815 378.
816 Daher, A., Laraki, G., Singh, M., Melendez-Peña, C.E., Bannwarth, S., Peters, A.H.F.M.,
817 Meurs, E.F., Braun, R.E., Patel, R.C., and Gatignol, A. (2009). TRBP control of PACT-
818 induced phosphorylation of protein kinase R is reversed by stress. Mol. Cell. Biol. *29*, 254–
819 265.
820 Daniels, S.M., Melendez-Peña, C.E., Scarborough, R.J., Daher, A., Christensen, H.S., El Far,
821 M., Purcell, D.F.J., Lainé, S., and Gatignol, A. (2009). Characterization of the TRBP
822 domain required for dicer interaction and function in RNA interference. BMC Mol. Biol.
823 *10*, 38.
824 Donaszi-Ivanov, A., Mohorianu, I., Dalmay, T., and Powell, P.P. (2013). Small RNA Analysis
825 in Sindbis Virus Infected Human HEK293 Cells. PLoS ONE *8*, e84070.
826 Doyle, M., Badertscher, L., Jaskiewicz, L., Güttinger, S., Jurado, S., Hugenschmidt, T., Kutay,
827 U., and Filipowicz, W. (2013). The double-stranded RNA binding domain of human Dicer
828 functions as a nuclear localization signal. RNA N. Y. N *19*, 1238–1252.
829 Elde, N.C., Child, S.J., Geballe, A.P., and Malik, H.S. (2009). Protein kinase R reveals an
830 evolutionary model for defeating viral mimicry. Nature *457*, 485–489.
831 Fairman-Williams, M.E., Guenther, U.-P., and Jankowsky, E. (2010). SF1 and SF2 helicases:
832 family matters. Curr. Opin. Struct. Biol. *20*, 313–324.
833 Fros, J.J., and Pijlman, G.P. (2016). Alphavirus Infection: Host Cell Shut-Off and Inhibition of
834 Antiviral Responses. Viruses *8*, 166.
835 Fujii, R., Okamoto, M., Aratani, S., Oishi, T., Ohshima, T., Taira, K., Baba, M., Fukamizu, A.,
836 and Nakajima, T. (2001). A Role of RNA Helicase A in cis-Acting Transactivation
837 Response Element-mediated Transcriptional Regulation of Human Immunodeficiency
838 Virus Type 1. J. Biol. Chem. *276*, 5445–5451.
839 Gal-Ben-Ari, S., Barrera, I., Ehrlich, M., and Rosenblum, K. (2018). PKR: A Kinase to
840 Remember. Front. Mol. Neurosci. *11*, 480.
841 García, M.A., Meurs, E.F., and Esteban, M. (2007). The dsRNA protein kinase PKR: Virus and
842 cell control. Biochimie *89*, 799–811.
843 Girardi, E., Chane-Woon-Ming, B., Messmer, M., Kaukinen, P., and Pfeffer, S. (2013).
844 Identification of RNase L-dependent, 3'-end-modified, viral small RNAs in Sindbis virus-
845 infected mammalian cells. MBio *4*, e00698-00613.
846 Girardi, E., Lefèvre, M., Chane-Woon-Ming, B., Paro, S., Claydon, B., Imler, J.-L., Meignin,
847 C., and Pfeffer, S. (2015). Cross-species comparative analysis of Dicer proteins during
848 Sindbis virus infection. Sci. Rep. *5*, 10693.
849 Griffin, D. (2007). Alphaviruses, p 1023–1067. Fields Virol. 5th Ed Lippincott Williams
850 Wilkins Phila. PA.
851 Guo, Z., Li, Y., and Ding, S.-W. (2019). Small RNA-based antimicrobial immunity. Nat. Rev.
852 Immunol. *19*, 31–44.
853 Haase, A.D., Jaskiewicz, L., Zhang, H., Laine, S., Sack, R., Gatignol, A., and Filipowicz, W.
854 (2005). TRBP, a regulator of cellular PKR and HIV-1 virus expression, interacts with Dicer
855 and functions in RNA silencing. EMBO Rep *6*, 961–967.
856 Herbert, A., Alfken, J., Kim, Y.G., Mian, I.S., Nishikura, K., and Rich, A. (1997). A Z-DNA
857 binding domain present in the human editing enzyme, double-stranded RNA adenosine
858 deaminase. Proc. Natl. Acad. Sci. U. S. A. *94*, 8421–8426.

859 Heyam, A., Lagos, D., and Plevin, M. (2015). Dissecting the roles of TRBP and PACT in
860 double-stranded RNA recognition and processing of noncoding RNAs. WIREs RNA *6*,
861 271–289.
862 Hutvágner, G., McLachlan, J., Pasquinelli, A.E., Balint, E., Tuschl, T., and Zamore, P.D.
863 (2001). A cellular function for the RNA-interference enzyme Dicer in the maturation of
864 the let-7 small temporal RNA. Science *293*, 834–838.
865 Iizasa, H., Wulff, B.-E., Alla, N.R., Maragkakis, M., Megraw, M., Hatzigeorgiou, A., Iwakiri,
866 D., Takada, K., Wiedmer, A., Showe, L., et al. (2010). Editing of Epstein-Barr virus-
867 encoded BART6 microRNAs controls their dicer targeting and consequently affects viral
868 latency. J. Biol. Chem. *285*, 33358–33370.
869 Ivashkiv, L.B., and Donlin, L.T. (2014). Regulation of type I interferon responses. Nat. Rev.
870 Immunol. *14*, 36–49.
871 Kennedy, E.M., Whisnant, A.W., Kornepati, A.V.R., Marshall, J.B., Bogerd, H.P., and Cullen,
872 B.R. (2015). Production of functional small interfering RNAs by an amino-terminal
873 deletion mutant of human Dicer. Proc. Natl. Acad. Sci. *112*, E6945–E6954.
874 Kim, Y., Lee, J.H., Park, J.-E., Cho, J., Yi, H., and Kim, V.N. (2014). PKR is activated by
875 cellular dsRNAs during mitosis and acts as a mitotic regulator. Genes Dev. *28*, 1310–1322.
876 Kok, K.H., Ng, M.H., Ching, Y.P., and Jin, D.Y. (2007). Human TRBP and PACT Directly
877 Interact with Each Other and Associate with Dicer to Facilitate the Production of Small
878 Interfering RNA. J Biol Chem *282*, 17649–17657.
879 Kok, K.-H., Lui, P.-Y., Ng, M.-H.J., Siu, K.-L., Au, S.W.N., and Jin, D.-Y. (2011). The Double-
880 Stranded RNA-Binding Protein PACT Functions as a Cellular Activator of RIG-I to
881 Facilitate Innate Antiviral Response. Cell Host Microbe *9*, 299–309.
882 Kuleshov, M.V., Jones, M.R., Rouillard, A.D., Fernandez, N.F., Duan, Q., Wang, Z., Koplev,
883 S., Jenkins, S.L., Jagodnik, K.M., Lachmann, A., et al. (2016). Enrichr: a comprehensive
884 gene set enrichment analysis web server 2016 update. Nucleic Acids Res. *44*, W90-97.
885 Lambert, M., Pépin, G., Peralta-Zaragoza, O., Matusiak, R., Ly, S., Landry, P., and Provost, P.
886 (2016). TWEAK Negatively Regulates Human Dicer. Non-Coding RNA *2*.
887 Lee, Y., Hur, I., Park, S.Y., Kim, Y.K., Suh, M.R., and Kim, V.N. (2006). The role of PACT
888 in the RNA silencing pathway. Embo J *25*, 522–532.
889 Lemaire, P.A., Anderson, E., Lary, J., and Cole, J.L. (2008). Mechanism of PKR Activation by
890 dsRNA. J. Mol. Biol. *381*, 351–360.
891 Lepur, A., Kovačević, L., Belužić, R., and Vugrek, O. (2016). Combining unique multiplex
892 gateway cloning and bimolecular fluorescence complementation (BiFC) for high-
893 throughput screening of protein–protein interactions. J. Biomol. Screen. *21*, 1100–1111.
894 Li, J., Tang, H., Mullen, T.M., Westberg, C., Reddy, T.R., Rose, D.W., and Wong-Staal, F.
895 (1999). A role for RNA helicase A in post-transcriptional regulation of HIV type 1. Proc.
896 Natl. Acad. Sci. U. S. A. *96*, 709–714.
897 Li, Y., Lu, J., Han, Y., Fan, X., and Ding, S.-W. (2013). RNA interference functions as an
898 antiviral immunity mechanism in mammals. Science *342*, 231–234.
899 Li, Y., Basavappa, M., Lu, J., Dong, S., Cronkite, D.A., Prior, J.T., Reinecker, H.-C., Hertzog,
900 P., Han, Y., Li, W.-X., et al. (2016). Induction and suppression of antiviral RNA
901 interference by influenza A virus in mammalian cells. Nat. Microbiol. *2*, 16250.
902 Li, Z., Wolff, K.C., and Samuel, C.E. (2010). RNA adenosine deaminase ADAR1 deficiency
903 leads to increased activation of protein kinase PKR and reduced vesicular stomatitis virus
904 growth following interferon treatment. Virology *396*, 316–322.
905 Lui, P.-Y., Wong, L.-Y.R., Ho, T.-H., Au, S.W.N., Chan, C.-P., Kok, K.-H., and Jin, D.-Y.
906 (2017). PACT Facilitates RNA-Induced Activation of MDA5 by Promoting MDA5
907 Oligomerization. J. Immunol. *199*, 1846–1855.

908 Maillard, P.V., Ciaudo, C., Marchais, A., Li, Y., Jay, F., Ding, S.W., and Voinnet, O. (2013).
909 Antiviral RNA interference in mammalian cells. Science *342*, 235–238.
910 Maillard, P.V., Veen, A.G.V. der, Deddouche-Grass, S., Rogers, N.C., Merits, A., and Sousa,
911 C.R. e (2016). Inactivation of the type I interferon pathway reveals long double-stranded
912 RNA-mediated RNA interference in mammalian cells. EMBO J. *35*, 2505–2518.
913 Maillard, P.V., van der Veen, A.G., Poirier, E.Z., and Reis e Sousa, C. (2019). Slicing and
914 dicing viruses: antiviral RNA interference in mammals. EMBO J. *38*.
915 Meister, G., and Tuschl, T. (2004). Mechanisms of gene silencing by double-stranded RNA.
916 Nature *431*, 343–349.
917 Meister, G., Landthaler, M., Peters, L., Chen, P.Y., Urlaub, H., Lührmann, R., and Tuschl, T.
918 (2005). Identification of novel argonaute-associated proteins. Curr. Biol. CB *15*, 2149–
919 2155.
920 Mittelstadt, M., Frump, A., Khuu, T., Fowlkes, V., Handy, I., Patel, C.V., and Patel, R.C.
921 (2008). Interaction of human tRNA-dihydrouridine synthase-2 with interferon-induced
922 protein kinase PKR. Nucleic Acids Res. *36*, 998–1008.
923 Nakamura, T., Kunz, R.C., Zhang, C., Kimura, T., Yuan, C.L., Baccaro, B., Namiki, Y., Gygi,
924 S.P., and Hotamisligil, G.S. (2015). A Critical Role for PKR Complexes with TRBP in
925 Immunometabolic Regulation and eIF2α Phosphorylation in Obesity. Cell Rep. *11*, 295–
926 307.
927 Ota, H., Sakurai, M., Gupta, R., Valente, L., Wulff, B.-E., Ariyoshi, K., Iizasa, H., Davuluri,
928 R.V., and Nishikura, K. (2013). ADAR1 forms a complex with Dicer to promote
929 microRNA processing and RNA-induced gene silencing. Cell *153*, 575–589.
930 Parameswaran, P., Sklan, E., Wilkins, C., Burgon, T., Samuel, M.A., Lu, R., Ansel, K.M.,
931 Heissmeyer, V., Einav, S., Jackson, W., et al. (2010). Six RNA viruses and forty-one hosts:
932 viral small RNAs and modulation of small RNA repertoires in vertebrate and invertebrate
933 systems. PLoS Pathog *6*, e1000764.
934 Park, H., Davies, M.V., Langland, J.O., Chang, H.W., Nam, Y.S., Tartaglia, J., Paoletti, E.,
935 Jacobs, B.L., Kaufman, R.J., and Venkatesan, S. (1994). TAR RNA-binding protein is an
936 inhibitor of the interferon-induced protein kinase PKR. Proc. Natl. Acad. Sci. U. S. A. *91*,
937 4713–4717.
938 Patel, C.V., Handy, I., Goldsmith, T., and Patel, R.C. (2000). PACT, a Stress-modulated
939 Cellular Activator of Interferon-induced Double-stranded RNA-activated Protein Kinase,
940 PKR. J. Biol. Chem. *275*, 37993–37998.
941 Perez-Riverol, Y., Csordas, A., Bai, J., Bernal-Llinares, M., Hewapathirana, S., Kundu, D.J.,
942 Inuganti, A., Griss, J., Mayer, G., Eisenacher, M., et al. (2019). The PRIDE database and
943 related tools and resources in 2019: improving support for quantification data. Nucleic
944 Acids Res. *47*, D442–D450.
945 Pfaller, C.K., Li, Z., George, C.X., and Samuel, C.E. (2011). Protein kinase PKR and RNA
946 adenosine deaminase ADAR1: new roles for old players as modulators of the interferon
947 response. Curr. Opin. Immunol. *23*, 573–582.
948 Qiu, Y., Xu, Y., Zhang, Y., Zhou, H., Deng, Y.-Q., Li, X.-F., Miao, M., Zhang, Q., Zhong, B.,
949 Hu, Y., et al. (2017). Human Virus-Derived Small RNAs Can Confer Antiviral Immunity
950 in Mammals. Immunity *46*, 992-1004.e5.
951 Qiu, Y., Xu, Y.-P., Wang, M., Miao, M., Zhou, H., Xu, J., Kong, J., Zheng, D., Li, R.-T., and
952 Zhang, R.-R. (2020). Flavivirus induces and antagonizes antiviral RNA interference in both
953 mammals and mosquitoes. Sci. Adv. *6*, eaax7989.
954 Robb, G.B., and Rana, T.M. (2007). RNA helicase A interacts with RISC in human cells and
955 functions in RISC loading. Mol. Cell *26*, 523–537.

Roy, B.B., Hu, J., Guo, X., Russell, R.S., Guo, F., Kleiman, L., and Liang, C. (2006). Association of RNA helicase a with human immunodeficiency virus type 1 particles. J. Biol. Chem. *281*, 12625–12635.

Ryman, K.D., White, L.J., Johnston, R.E., and Klimstra, W.B. (2002). Effects of PKR/RNase L-Dependent and Alternative Antiviral Pathways on Alphavirus Replication and Pathogenesis. Viral Immunol. *15*, 53–76.

Sadler, A.J., Latchoumanin, O., Hawkes, D., Mak, J., and Williams, B.R.G. (2009). An Antiviral Response Directed by PKR Phosphorylation of the RNA Helicase A. PLoS Pathog. *5*, e1000311.

Samuel, C.E. (2011). Adenosine deaminases acting on RNA (ADARs) are both antiviral and proviral. Virology *411*, 180–193.

Schoggins, J.W., Wilson, S.J., Panis, M., Murphy, M.Y., Jones, C.T., Bieniasz, P., and Rice, C.M. (2011). A diverse range of gene products are effectors of the type I interferon antiviral response. Nature *472*, 481–485.

Schuster, S., Overheul, G.J., Bauer, L., van Kuppeveld, F.J.M., and van Rij, R.P. (2019). No evidence for viral small RNA production and antiviral function of Argonaute 2 in human cells. Sci. Rep. *9*, 1–11.

Singh, M., Castillo, D., Patel, C.V., and Patel, R.C. (2011). Stress-induced phosphorylation of PACT reduces its interaction with TRBP and leads to PKR activation. Biochemistry *50*, 4550–4560.

Takahashi, T., and Ui-Tei, K. (2020). Mutual Regulation of RNA Silencing and the IFN Response as an Antiviral Defense System in Mammalian Cells. Int. J. Mol. Sci. *21*, 1348.

Takahashi, T., Nakano, Y., Onomoto, K., Murakami, F., Komori, C., Suzuki, Y., Yoneyama, M., and Ui-Tei, K. (2018a). LGP2 virus sensor regulates gene expression network mediated by TRBP-bound microRNAs. Nucleic Acids Res. *46*, 9134–9147.

Takahashi, T., Nakano, Y., Onomoto, K., Yoneyama, M., and Ui-Tei, K. (2018b). Virus Sensor RIG-I Represses RNA Interference by Interacting with TRBP through LGP2 in Mammalian Cells. Genes *9*, 511.

tenOever, B.R. (2016). The Evolution of Antiviral Defense Systems. Cell Host Microbe *19*, 142–149.

Tsai, K., Courtney, D.G., Kennedy, E.M., and Cullen, B.R. (2018). Influenza A virus-derived siRNAs increase in the absence of NS1 yet fail to inhibit virus replication. RNA N. Y. N.

van der Veen, A.G., Maillard, P.V., Schmidt, J.M., Lee, S.A., Deddouche-Grass, S., Borg, A., Kjær, S., Snijders, A.P., and Reis e Sousa, C. (2018). The RIG-I-like receptor LGP2 inhibits Dicer-dependent processing of long double-stranded RNA and blocks RNA interference in mammalian cells. EMBO J. *37*, e97479.

Wienholds, E., Koudijs, M.J., Van Eeden, F.J., Cuppen, E., and Plasterk, R.H. (2003). The microRNA-producing enzyme Dicer1 is essential for zebrafish development. Nat Genet 217–218.

Williams, B.R. (1999). PKR; a sentinel kinase for cellular stress. Oncogene *18*, 6112–6120.

Yang, W., Chendrimada, T.P., Wang, Q., Higuchi, M., Seeburg, P.H., Shiekhattar, R., and Nishikura, K. (2006). Modulation of microRNA processing and expression through RNA editing by ADAR deaminases. Nat Struct Mol Biol *13*, 13–21.

Figure legends

Figure 1. Analysis of SINV infection in HEK293T cells and characterization of FHA:DICER WT cell lines.

A. GFP fluorescent microscopy pictures of HEK293T, NoDice FHA:ctrl #1 and FHA:DICER cell lines infected (polyclonal and two clones, #4 and #17) with SINV-GFP at an MOI of 0.02 for 24 h. The left panel corresponds to GFP signal from infected cells and the right panel to a merge picture of GFP signal and brightfield. Pictures were taken with a 5x magnification. hpi: hours post-infection. **B.** Western blot analysis of DICER (DICER and HA) and GFP expression in SINV-GFP-infected HEK293T, NoDice FHA:ctrl #1 and FHA:DICER cell lines shown in **A**. Gamma-Tubulin was used as loading control. **C.** Mean (+/- SEM) of SINV-GFP viral titers in the same cell lines as in **A** infected at an MOI of 0.02 for 24 h (n = 3) from plaque assay quantification. ns: non-significant, ordinary one-way ANOVA test with Bonferroni correction. **D.** Western blot analysis of DICER (DICER and HA) and AGO2 expression in HEK293T, NoDice FHA:ctrl #1 and FHA:DICER cell lines. Gamma-Tubulin was used as loading control.

Figure 2. LC-MS/MS analysis of DICER interactome during SINV infection.

A. Volcano plot for differentially expressed proteins (DEPs) between HA IP and CTL IP in FHA:DICER mock-infected cells. Each protein is marked as a dot; proteins that are significantly up-regulated in HA IP are shown in red, up-regulated proteins in CTL IP are shown in blue, and non-significant proteins are in black. The horizontal line denotes a p-value of 0.05 and the vertical lines the Log2 fold change cutoff (-1 and 1). DICER and its cofactors (TRBP, PACT, AGO2) are highlighted in yellow. **B.** Volcano plot for DEPs between SINV-GFP (MOI of 2, 6 hpi) and mock fractions of HA IP in FHA:DICER cells. Same colour code and thresholds as in A have been applied. Proteins that are discussed in the text are highlighted in yellow and SINV proteins in purple. **C.** Gene Ontology (GO) term enrichment of proteins

up-regulated in SINV-GFP fraction of HA IP using Enrichr software (Chen et al., 2013; Kuleshov et al., 2016). The graph displays the GO term hierarchy within the "biological process" branch sorted by p-value ranking computed from the Fisher exact test. The length of each bar represents the significance of that specific term. In addition, the brighter the colour is, the more significant that term is. Viral proteins have been excluded for this analysis. **D.** Summary of the differential expression analysis of SINV-GFP vs mock fractions from HA IP in FHA:DICER cells. The analysis has been performed using a generalized linear model of a negative-binomial distribution and p-values were corrected for multiple testing using the Benjamini-Hochberg method.

Figure 3. Confirmation of LC-MS/MS analysis by co-IP and BiFC.

A. Western blot analysis of HA co-IP in mock or SINV-GFP-infected (MOI of 2, 6 hpi) FHA:DICER WT #4 cells. Proteins associated to FHA:DICER were revealed by using antibodies targeting endogenous ADAR-1, PKR, TRBP, DHX9 or PACT proteins. In parallel, an HA antibody was used to verify the IP efficiency and GFP antibody was used to verify the infection. Ponceau was used as loading control. **B.** Western blot analysis of HA co-IP in mock or SINV-GFP-infected (MOI of 2, 6 hpi) FHA:DICER WT #4 cells. The lysate was treated or not with RNase A/T1. Proteins associated to FHA:DICER were revealed by using antibodies targeting endogenous DHX9, p-PKR, PKR, TRBP, or PACT proteins. In parallel, an HA antibody was used to verify the IP efficiency and GFP antibody was used to verify the infection. Ponceau was used as loading control. The arrow points to the expected size of the FHA:DICER protein and the asterisks correspond to aspecific bands. **C.** Western blot analysis to validate the interaction of PKR with DICER (upper panel) and PACT (lower panel) in mock or SINV-GFP-infected HEK293T cells. Immunoprecipitated proteins obtained from PKR pulldowns were compared to IgG pulldowns to verify the specificity of the assay. **D.** Interactions between

DICER and TRBP, PACT or PKR were visualized by BiFC. Plasmids expressing $^{N\text{-}ter}$Venus:DICER and TRBP:, PACT: or PKR:Venus$^{C\text{-}ter}$ were co-transfected in NoDice/ΔPKR cells for 24 h and cells were either infected with SINV at an MOI of 2 for 6 h or not. The different combinations are indicated on the left side. Reconstitution of Venus (BiFC) signal was observed under epifluorescence microscope. For each condition, the left panel corresponds to Venus signal and the right panel to the corresponding brightfield pictures. Scale bar: 100 μm. hpi: hours post-infection. **E.** BiFC experiment on fixed NoDice/ΔPKR cells treated as in D. After fixation, cells were stained with DAPI and observed under confocal microscope. Only a merge picture of BiFC and DAPI signals of SINV-infected cells is shown here. A higher magnification of picture showing cytoplasmic localization of the interaction represented by a red square is shown in the bottom left corner. Scale bar: 20 μm and 10 μm.

Figure 4. Confirmation of DICER interactome upon SINV infection in HCT116 KI-DICER cells.

A. Western blot analysis of DICER, AGO2, PKR and TRBP expression in HEK293T, HCT116 and HCT116 KI-DICER cell lines. Gamma-Tubulin and ponceau were used as loading control. **B**. GFP fluorescent microscopy pictures of HEK293T, HCT116 and HCT116 KI-DICER cell lines infected with SINV-GFP at an MOI of 0.02, 0.1 and 1 for 24 h. The left panel corresponds to GFP signal from infected cells and the right panel to a merge picture of GFP signal and brightfield. Pictures were taken with a 5x magnification. **C**. miR-16 expression analyzed by northern blot in in the same cell lines as in B. Expression of snRNA U6 was used as loading control. **D.** Western blot analysis of HA co-IP in mock or SINV-GFP-infected (MOI of 0.1, 24 hpi) HCT116 KI-DICER cells. Proteins associated to FHA-GFP:DICER were revealed by using antibodies targeting endogenous DHX9, p-PKR, PKR, PACT or TRBP proteins. In parallel, an

HA antibody was used to verify the IP efficiency and GFP antibody was used to verify the infection. Ponceau was used as loading control.

Figure 5. Identification of DICER domains involved in DICER-PKR interaction.

A. Schematic representation of Human DICER proteins used in this study. The different conserved domains are shown in colored boxes. DUF283: Domain of Unknown Function; PAZ: PIWI ARGONAUTE ZWILLE domain; dsRBD: dsRNA-binding domain. hDICER WT is the full-length protein. hDICER N1 is deleted of the first N-terminal 495 amino acids. hDICER N3 is wholly deleted of the helicase domain. hDICER Hel. is the whole DICER's helicase domain. hDICER ΔdsRBD is deleted of the C-terminal dsRBD. **B.** Western blot analysis of HA co-IP in mock NoDice 2.20 cells transfected with different versions of FHA:DICER proteins. Efficiency of immunoprecipitation was assessed using anti-HA and anti-DICER antibodies and co-IPs of TRBP, PKR and PACT were examined using appropriate antibodies. Expression of GFP in INPUT fraction was visualized as control of SINV-GFP infection. Ponceau staining of membranes is used as loading control. **C.** Western blot analysis of HA co-IP in NoDice 2.20 cells transfected with different versions of FHA:DICER proteins and infected with SINV-GFP (MOI of 2, 6 hpi). Efficiency of immunoprecipitation was assessed using an anti- Flag antibody and co-IPs of PKR, TRBP, p-PKR and PACT were examined using appropriate antibodies. Expression of GFP in INPUT fraction was visualized as control of SINV-GFP infection. Ponceau staining of membranes is used as loading control. **D.** Plasmids expressing the different versions of DICER proteins fused to the N-terminal part of Venus and PKR:Venus$^{C\text{-}ter}$ plasmid were co-transfected in NoDice/ΔPKR cells. Cells were treated as in Fig. 3D. The different combinations are noted on the left side. The fluorescent signal was observed using an epifluorescence microscope. For each condition, the left panel corresponds to Venus signal and

1099 the right panel to the corresponding brightfield pictures. Scale bar: 100 µm. hpi: hours post-
1100 infection.
1101
1102 **Figure 6. Analysis of the importance of Dicer helicase domain on SINV-GFP infection in**
1103 **FHA:DICER mutant stable cell lines.**
1104 **A.** Expression of DICER (DICER, HA), TRBP and AGO2 was analysed by western blot in
1105 HEK293T, NoDice FHA:ctrl #1, FHA:DICER WT #4 and FHA:DICER N1 #6 cell lines.
1106 Gamma-Tubulin was used as loading control. **B.** Northern blot analysis of miR-16 expression
1107 in the same samples as in A. Expression of snRNA U6 was used as loading control. **C.**
1108 Representative GFP fluorescent microscopy images of HEK293T, FHA:DICER WT #4 and
1109 FHA:DICER N1 #6 cell lines infected with SINV-GFP at an MOI of 0.02 for 24 h. The left
1110 panel corresponds to GFP signal and the right panel to a merge picture of GFP signal and
1111 brightfield. Pictures were taken with a 5x magnification. hpi: hours post-infection. **D.** Western
1112 blot analysis of DICER (DICER and HA), AGO2, PKR, and GFP expression in SINV-GFP-
1113 infected cells in the same condition as in C. Gamma-Tubulin was used as loading control. The
1114 asterisk correspond to aspecific bands **E.** Mean (+/- SEM) of SINV-GFP viral titers fold change
1115 over HEK293T cells in HEK293T, NoDice 2.20, FHA:DICER WT #4 and FHA:DICER
1116 mutants cell lines infected at an MOI of 0.02 for 24 h (n = 3) from plaque assay quantification.
1117 * $p < 0.05$, ns: non-significant, ordinary one-way ANOVA test with Bonferroni correction.
1118

Supplementary material

Supplementary figure legends

Figure S1. Analysis of SINV-GFP infection in FHA:DICER cell lines at different MOI and time points.

A. miR-16 expression analyzed by northern blot in HEK293T, NoDice FHA:ctrl #1 and FHA:DICER WT #4 cell lines**.** Expression of snRNA U6 was used as loading control. **B.** Representative GFP pictures of HEK293T, NoDice 2.20, NoDice 4.25, NoDice FHA:ctrl #1 and NoDice FHA:ctrl #2 cells infected with SINV-GFP at an MOI of 0.02 for 24h. The left panel corresponds to GFP signal and the right panel to a merge of GFP signal and the corresponding brightfield. Pictures were taken with a 5x magnification. hpi: hours post-infection. **C.** Mean (+/- SEM) of SINV-GFP viral titers in cells infected at an MOI of 0.02 for 24 h (n=3) from plaque assay quantification. * $p < 0.05$, ns: non-significant, ordinary one-way ANOVA test with Bonferroni correction. **D**. Western blot analysis of DICER, AGO2 and GFP expression in SINV-GFP-infected cells shown in B. Gamma-Tubulin was used as loading control.

Figure S2. LC-MS/MS analysis of DICER interactome during SFV infection.

A. Volcano plot for differentially expressed proteins (DEPs) between HA IP and CTL IP in FHA:DICER mock-infected cells. Each protein is marked as a dot; proteins that are significantly up-regulated in HA IP are shown in red, up-regulated proteins in CTL IP are shown in blue, and non-significant proteins are in black. The horizontal line denotes a p-value of 0.05 and the vertical lines the Log2 fold change cutoff (-1 and 1). DICER and its cofactors (TRBP, PACT, AGO2) are highlighted in yellow. **B.** Left panel: Volcano plot for DEPs between SFV (MOI of 2, 6 hpi) and mock fractions of HA IP in FHA:DICER cells. Same colour

code and thresholds as in A were applied. Proteins that are discussed in the text are highlighted in yellow and SFV proteins in purple. **C.** Summary of the differential expression analysis of SFV vs mock fractions from HA IP in FHA:DICER cells. The analysis has been performed using a generalized linear model of a negative-binomial distribution and p-values were corrected for multiple testing using the Benjamini-Hochberg method.

Figure S3. Confirmation of LC-MS/MS analysis by co-IP and BiFC controls.

A. FHA:DICER WT #4 cells were infected with SINV-GFP at an MOI of 0.02 for 24 h and a HA co-IP was performed. Eluted proteins were resolved by western blot and IP efficiency was assessed using an HA antibody. In parallel, co-IPed proteins were visualized using appropriate antibodies. GFP antibody was used to verify the infection and Ponceau staining serves as loading control. **B.** 1% Agarose gel analysis of RNA extracted from INPUT of the co-IP in Fig. 3B. Ribosomal RNA integrity was compared to a control HEK293T cell line. RNAs were revealed using ethidium bromide under UV. **C.** Schematic representation of Human DICER proteins used for BiFC positive and negative controls. The different conserved domains are shown in colored boxes. DUF283: Domain of Unknown Function; PAZ: PIWI ARGONAUTE ZWILLE domain; dsRBD: dsRNA-binding domain. hDICER WT is the full-length protein. hDICER N1 is deleted of the first N-terminal 495 amino acids. **D.** Expression of BiFC plasmids was assessed by western blot. DICER proteins (WT and N1) and PKR were visualized using antibodies targeting endogenous proteins, whereas TRBP and PACT were detected using GFP antibody. Antibody targeting the SINV coat protein (CP) was used as infection control. Ponceau staining was used as loading control. **E.** Positive and negative BiFC controls on fixed NoDice/ΔPKR cells. After co-transfection, cells were infected with SINV at an MOI of 2 for 6 h and fixed. After fixation, cells were stained with DAPI and observed under confocal microscope. Merge pictures of BiFC and DAPI signals of SINV-infected cells are shown. A

higher magnification of images showing the interaction represented by a red square is shown in the bottom left corner. Scale bar: 20 μm and 10 μm. **F.** Expression of BiFC plasmids was assessed by western blot. DICER, PKR, TRBP and PACT were detected using GFP antibody. Antibody targeting the SINV coat protein (CP) was used as infection control. Gamma-Tubulin was used as loading control. The asterisk corresponds to an aspecific band. **G.** Interactions between DICER and TRBP, PACT or PKR were visualized by BiFC. Plasmids expressing $^{N\text{-}ter}$Venus:DICER and TRBP:, PACT: or PKR:Venus$^{C\text{-}ter}$ were co-transfected in HEK293T cells for 24 h and cells were either infected with SINV at an MOI of 2 for 6 h or not. The different combinations are indicated on the left side. Reconstitution of Venus (BiFC) signal was observed under epifluorescence microscope. For each condition, the left panel corresponds to Venus signal and the right panel to the corresponding brightfield pictures. Scale bar: 100 μm.

Figure S4. Confirmation of DICER interactome upon SINV infection in HCT116 KI-DICER cells.

A. Schematic representation of DICER WT and Flag-HA(FHA)-GFP kocked-in (KI) alleles. FHA sequence is in purple, GFP in green, DICER 5'UTR in orange and DICER coding region in yellow. The gRNA used to generate the KI was designed to target the first coding exon of DICER gene. **B.** PCR on genomic DNA extracted from WT and KI cells. **C.** An oligo outside the homologous recombination region and an oligo within the GFP tag were used to verify the presence of a 1040bp amplicon in HCT116 KI-DICER clone. Sequencing results corresponding to this region are shown. **D.** Western blot analysis of DICER, p-PKR, PKR and p-eIF2α expression in mock or SINVGFP-infected HEK293T and HCT116 KI-DICER cell lines at an MOI of 2 for 6h or 16h and 0.02 for 24h. GFP antibody was used to verify the infection. Ponceau and gamma-Tubulin were used as loading control.

Figure S5. Interaction analysis between the different versions of DICER and TRBP or PACT using BiFC assay.

NoDice/ΔPKR cells were co-transfected for 24 h with plasmids expressing the different versions of DICER proteins fused to the N-terminal part of Venus and either TRBP:Venus$^{C\text{-}ter}$ (**A**) or PACT:Venus$^{C\text{-}ter}$ (**B**). Cells were then infected with SINV at an MOI of 2 for 6 h and Venus signal was observed under epifluorescence microscope. The left panel corresponds to Venus signal and the right panel to the corresponding brightfield picture. Pictures were taken with a 5x magnification. hpi: hours post-infection. Scale bar: 100 μm.

Figure S6. Analysis of the importance of Dicer helicase domain on SINV-GFP infection in FHA:DICER mutant stable cell lines.

A. Northern blot analysis of miR-16 expression in HEK293T, NoDice 2.20, NoDice FHA:ctrl #2, FHA:DICER WT polyclonal, FHA:DICER N1 #6, FHA:DICER Hel. #2.6, and FHA:DICER N3 #2.13. Expression of snRNA U6 was used as loading control. **B.** Representative GFP fluorescent microscopy images of HEK293T, NoDice 2.20, FHA:DICER mutants cell lines infected with SINV-GFP at an MOI of 0.02 for 24 h. The left panel corresponds to GFP signal and the right panel to a merge picture of GFP signal and brightfield. Pictures were taken with a 5x magnification. hpi: hours post-infection. **C**. Mean (+/- SEM) of SINV-GFP viral titers over FHA:DICER WT #4 cells in FHA:DICER N1 #6, FHA:DICER N3 #2.13, NoDice FHA:ctrl #2 and NoDice 2.20 cell lines infected at an MOI of 0.02 for 24 h (n = 3) from plaque assay quantification. *** $p < 0.001$, ns: non-significant, ordinary one-way ANOVA test with Bonferroni correction.

Supplementary tables

Supp. Table 1: Top 100 proteins that are differentially immunoprecipitated in mock-infected FHA:DICER cells by the HA and Myc (CTL) antibodies. Related to Figure 2.

Supp. Table 2: Top 100 proteins that are differentially immunoprecipitated with the HA antibody in SINV-infected vs mock-infected FHA:DICER cells. Related to Figure 2.

Supp. Table 3: Top 100 proteins that are differentially immunoprecipitated in mock-infected FHA:DICER cells by the HA and Myc (CTL) antibodies, in the SFV infection experiment. Related to Figure S2.

Supp. Table 4: Top 100 proteins that are differentially immunoprecipitated with the HA antibody in SFV-infected vs mock-infected FHA:DICER cells. Related to Figure S2.

Supp. Table 5: List of primers used in this study.

Figure 1

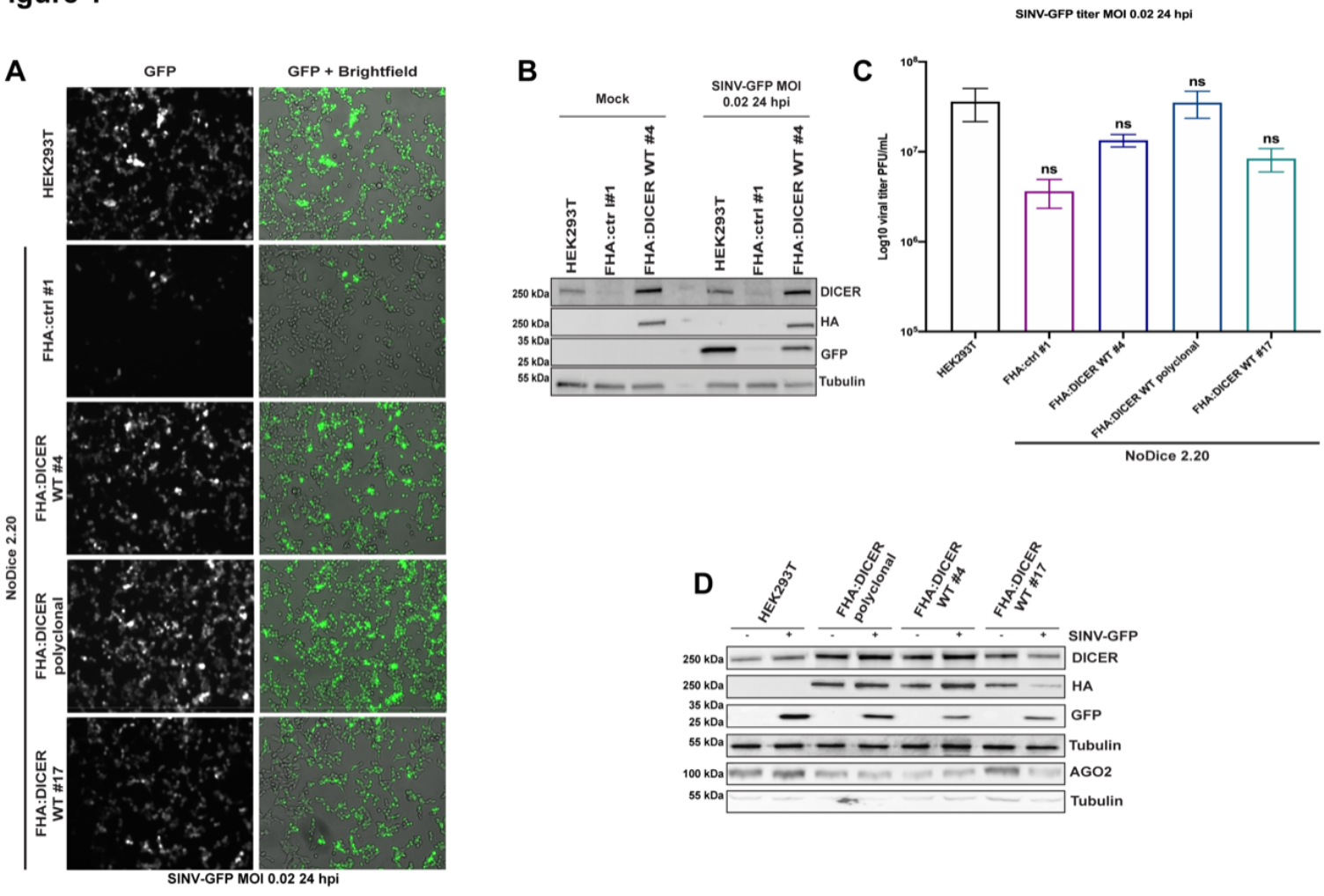

Figure 2

A

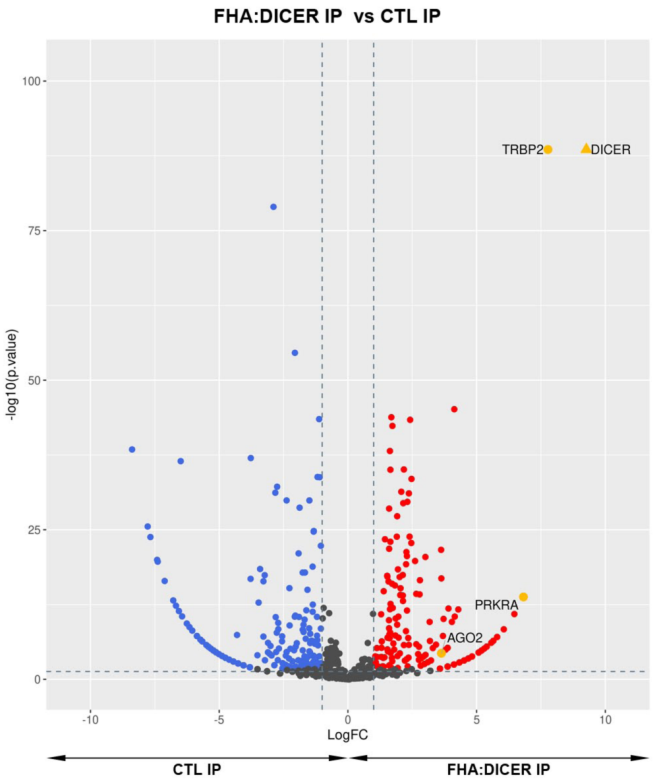

B

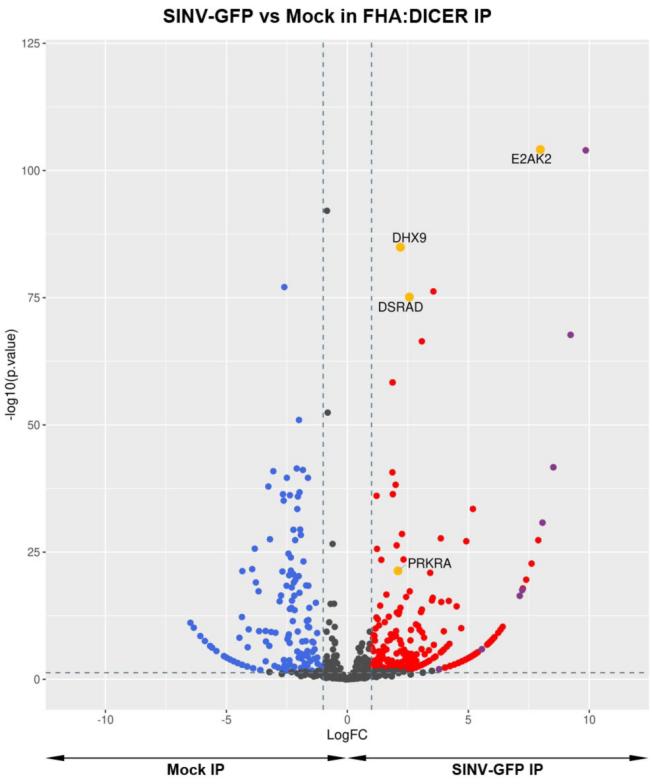

C

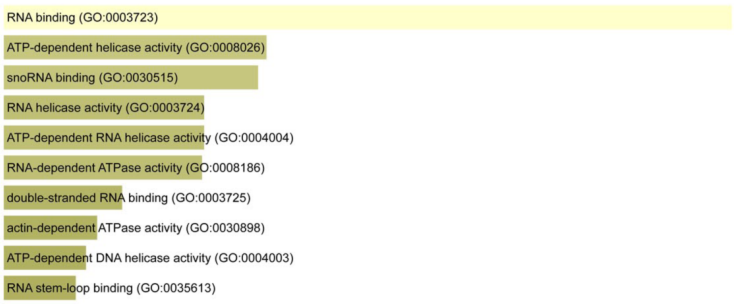

D

Gene name	Mean spectral count		LogFC	Adjusted p-value
	SINV-GFP IP	MOCK IP		
E2AK2 (PKR)	123.3	0.3	7.979	7.316e-102
DSRAD (ADAR-1)	181.3	28.3	2.563	1.421e-73
DHX9	247.3	50	2.194	4.012e-83
PRKRA (PACT)	63.3	13.7	2.093	1.158e-20

Figure 3

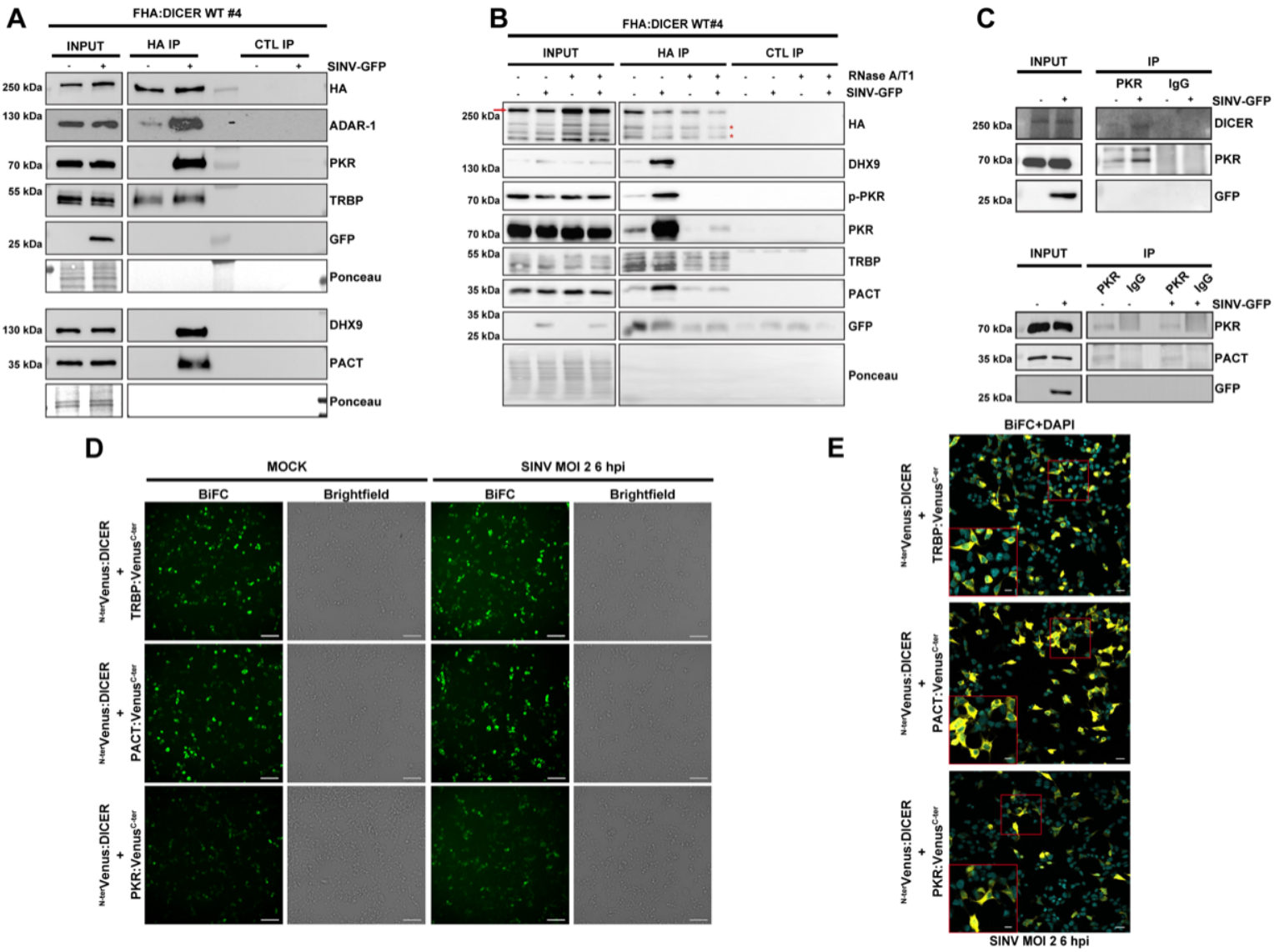

Figure 4

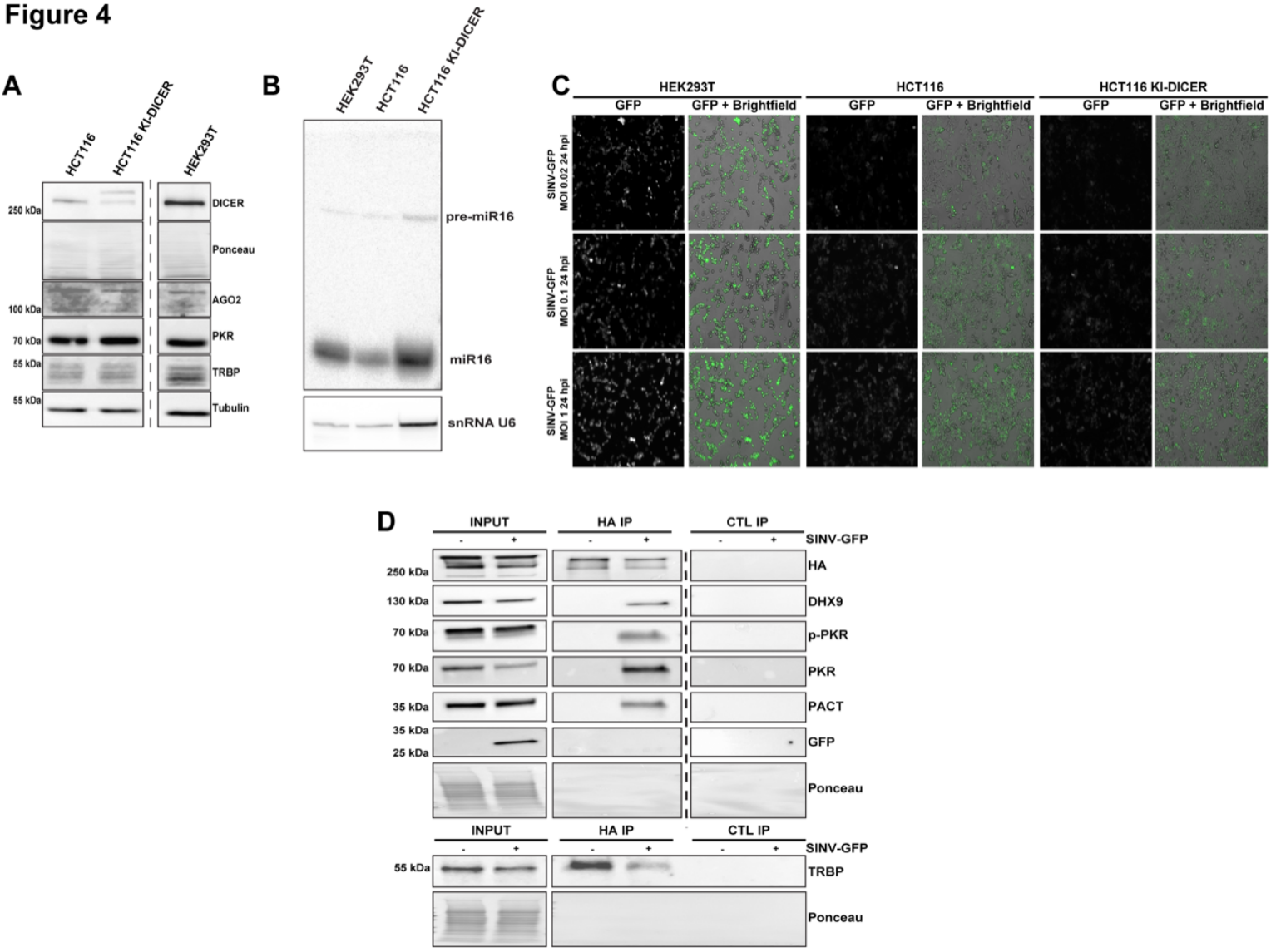

Figure 5

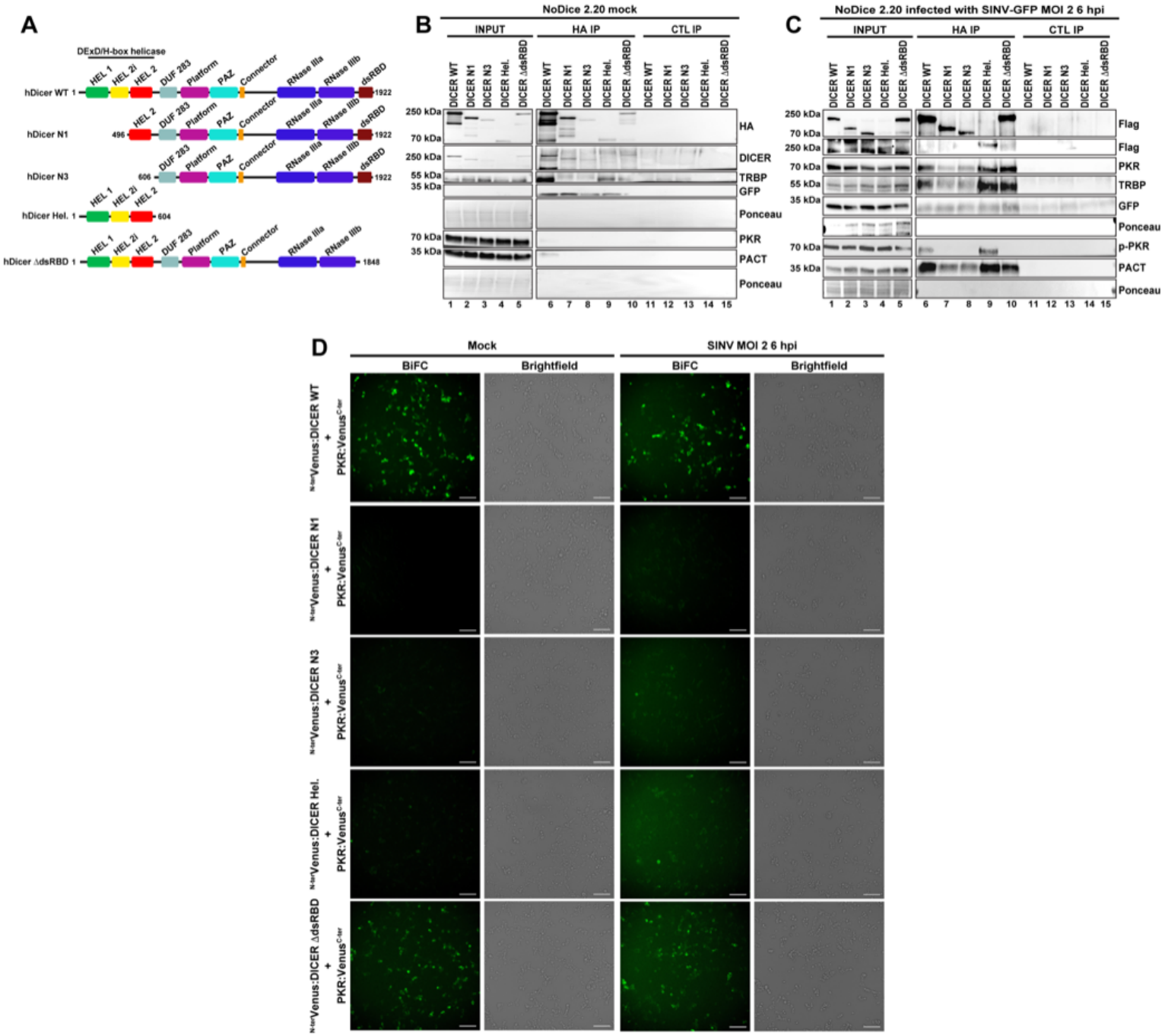

Figure 6

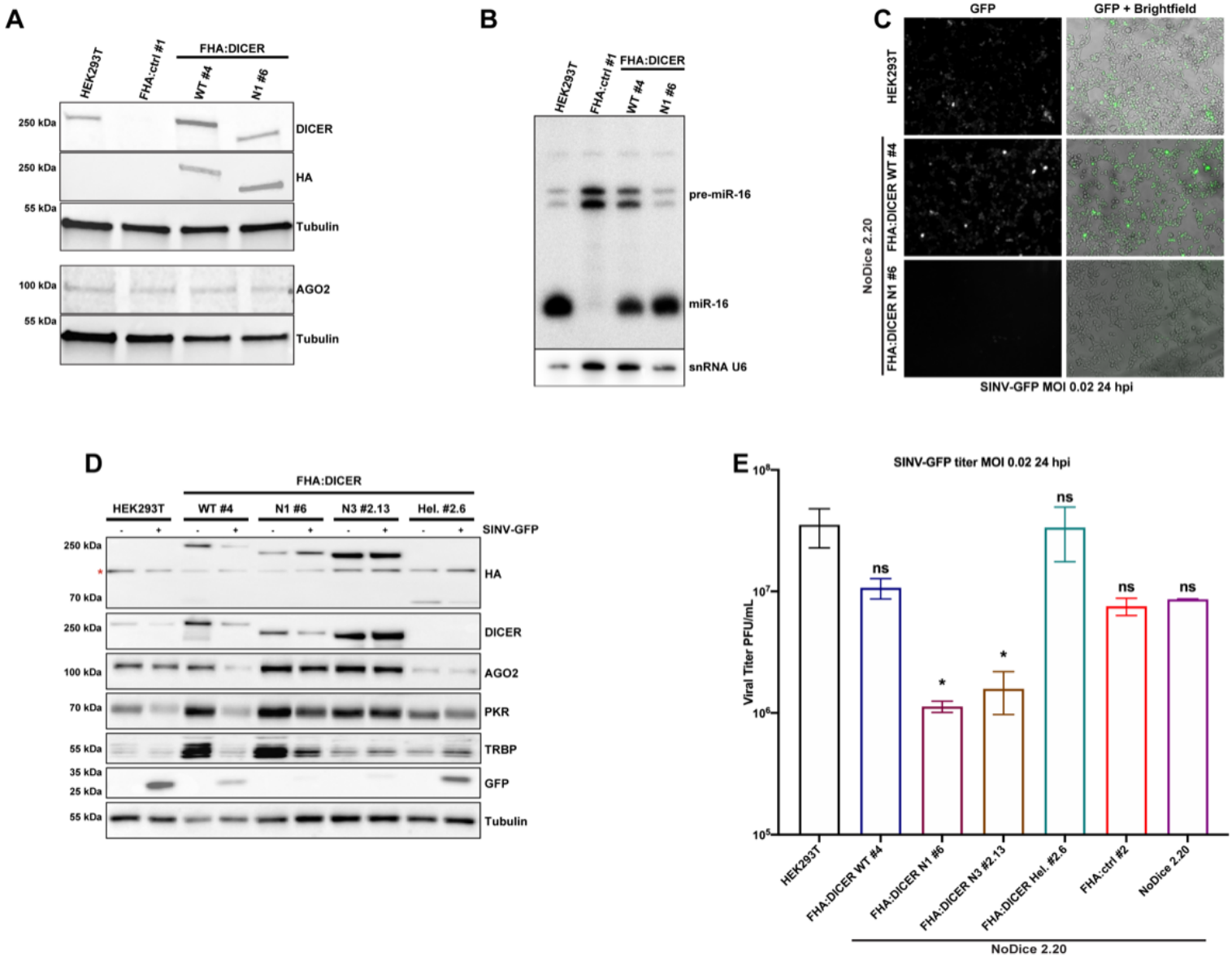

Figure S1

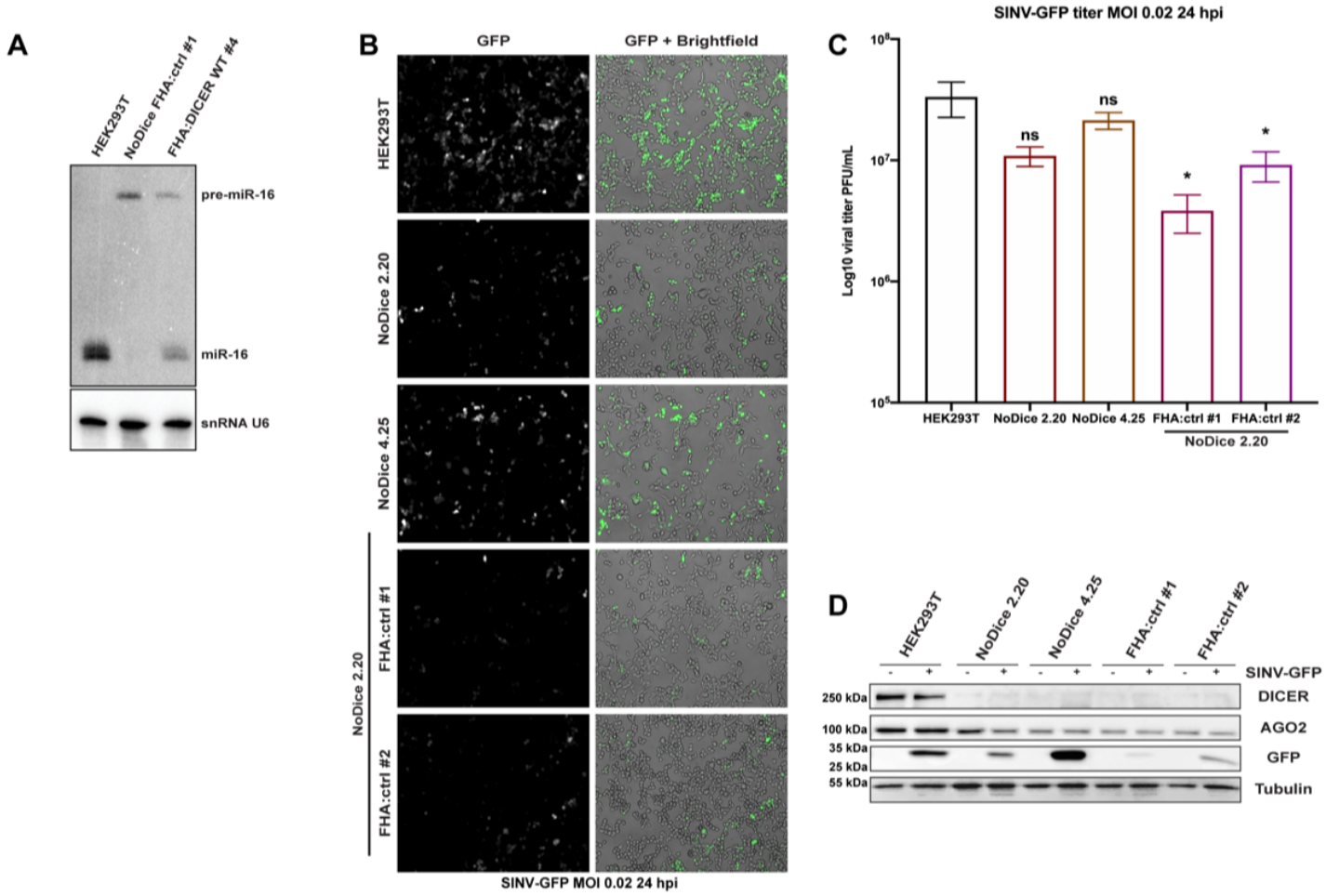

Figure S2

A

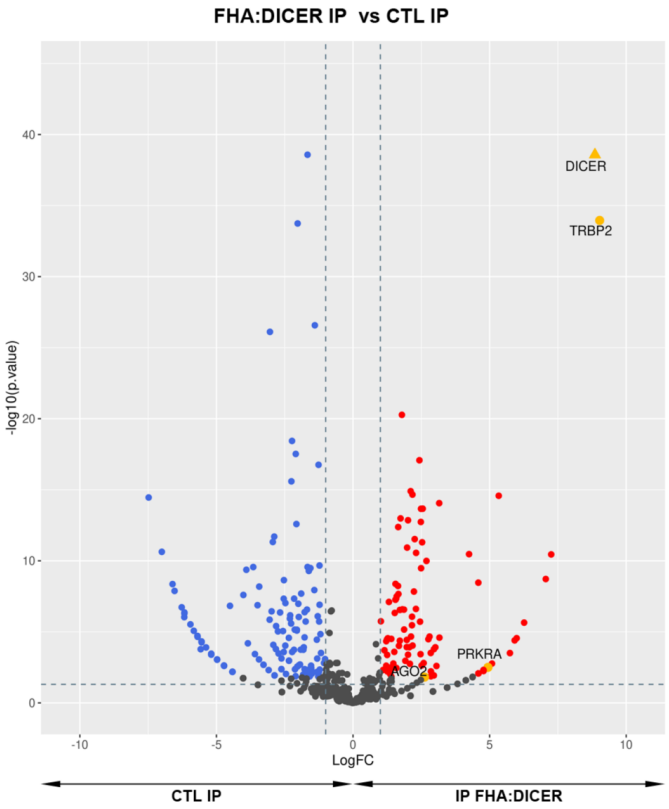

B

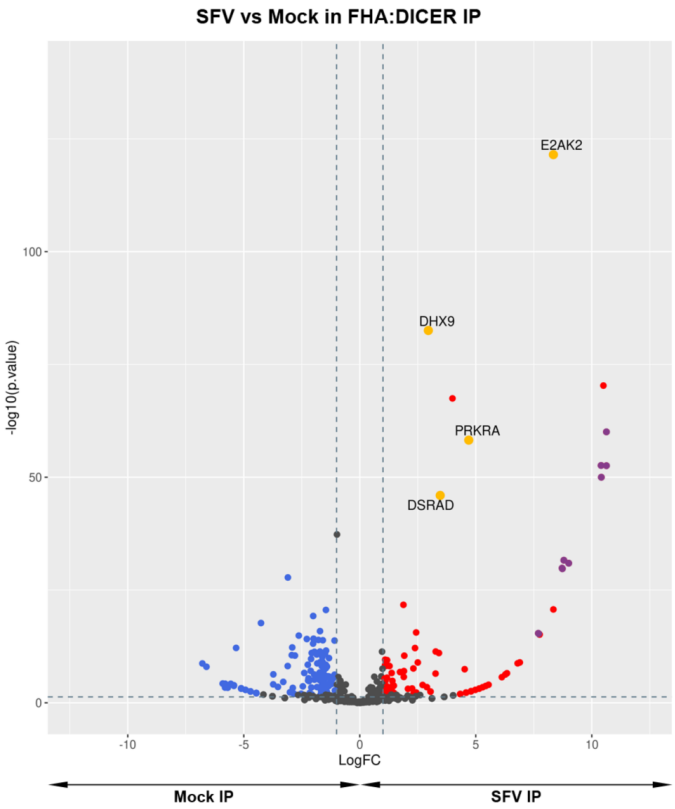

C

Gene name	Mean spectral count		LogFC	Adjusted p-value
	SFV IP	Mock IP		
E2AK2 (PKR)	221	0.5	8.344	2.611e-119
PRKRA (PACT)	131.5	4.5	4.697	8.415e-57
DSRAD (ADAR-1)	268	22	3.466	9.118e-45
DHX9	265	31	2.955	1.245e-80

Figure S3

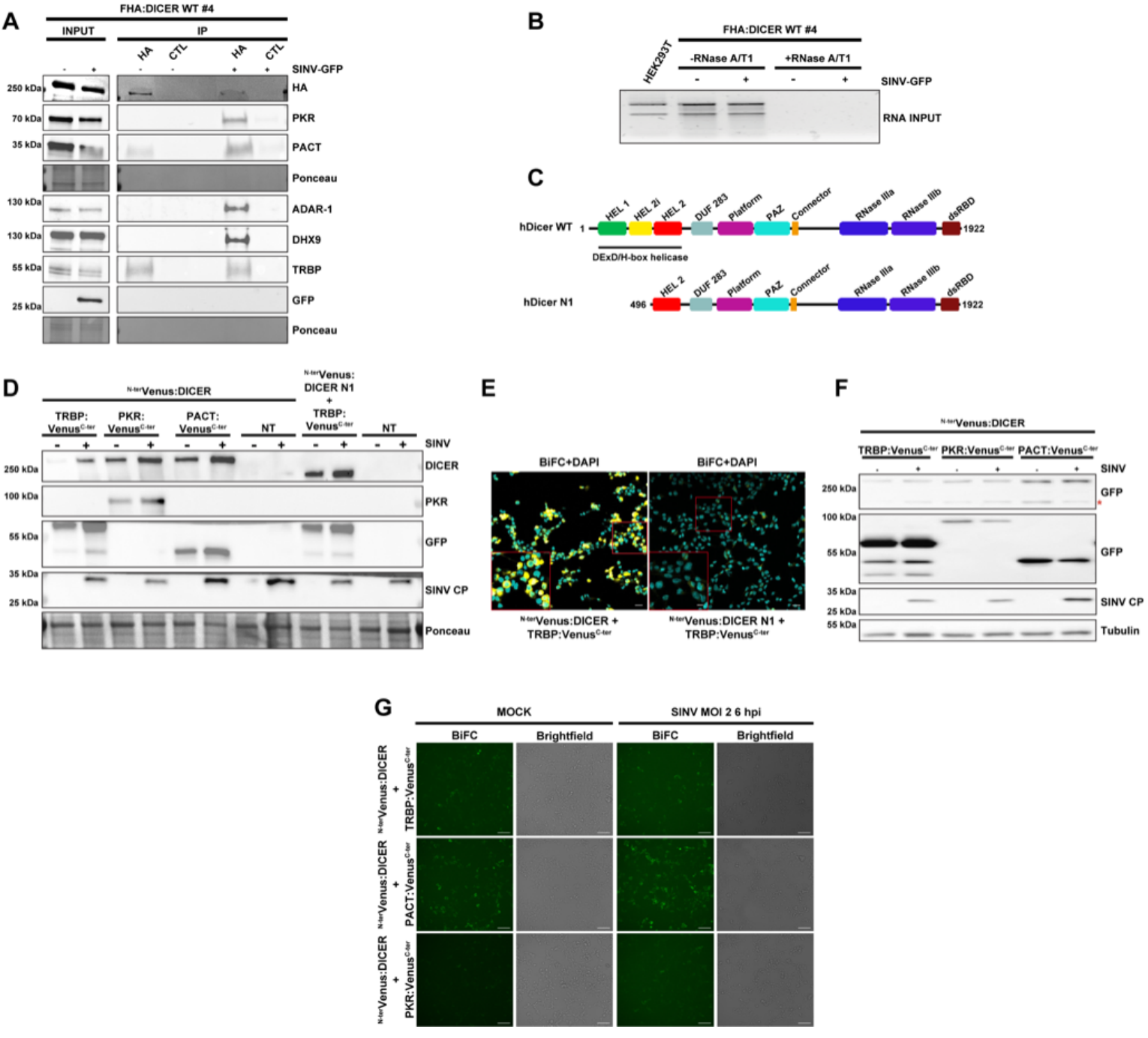

Figure S4

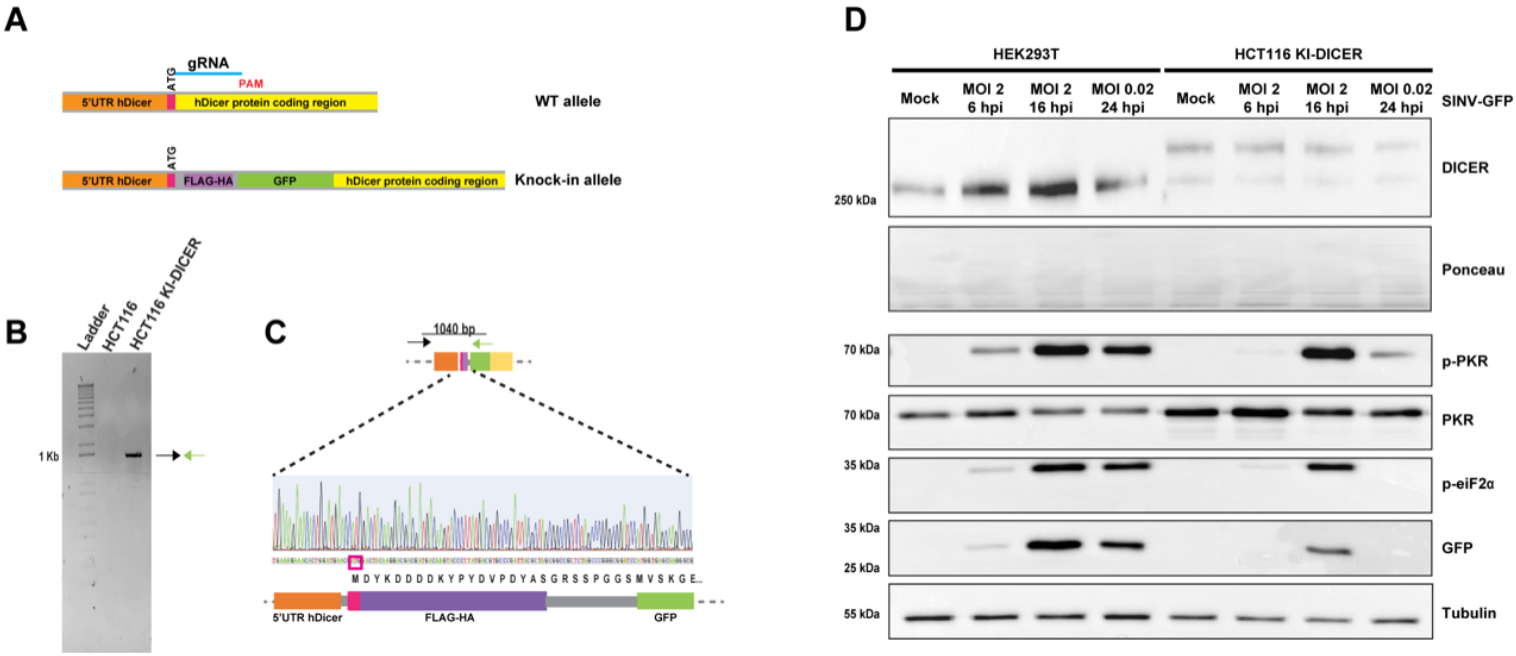

Figure S5

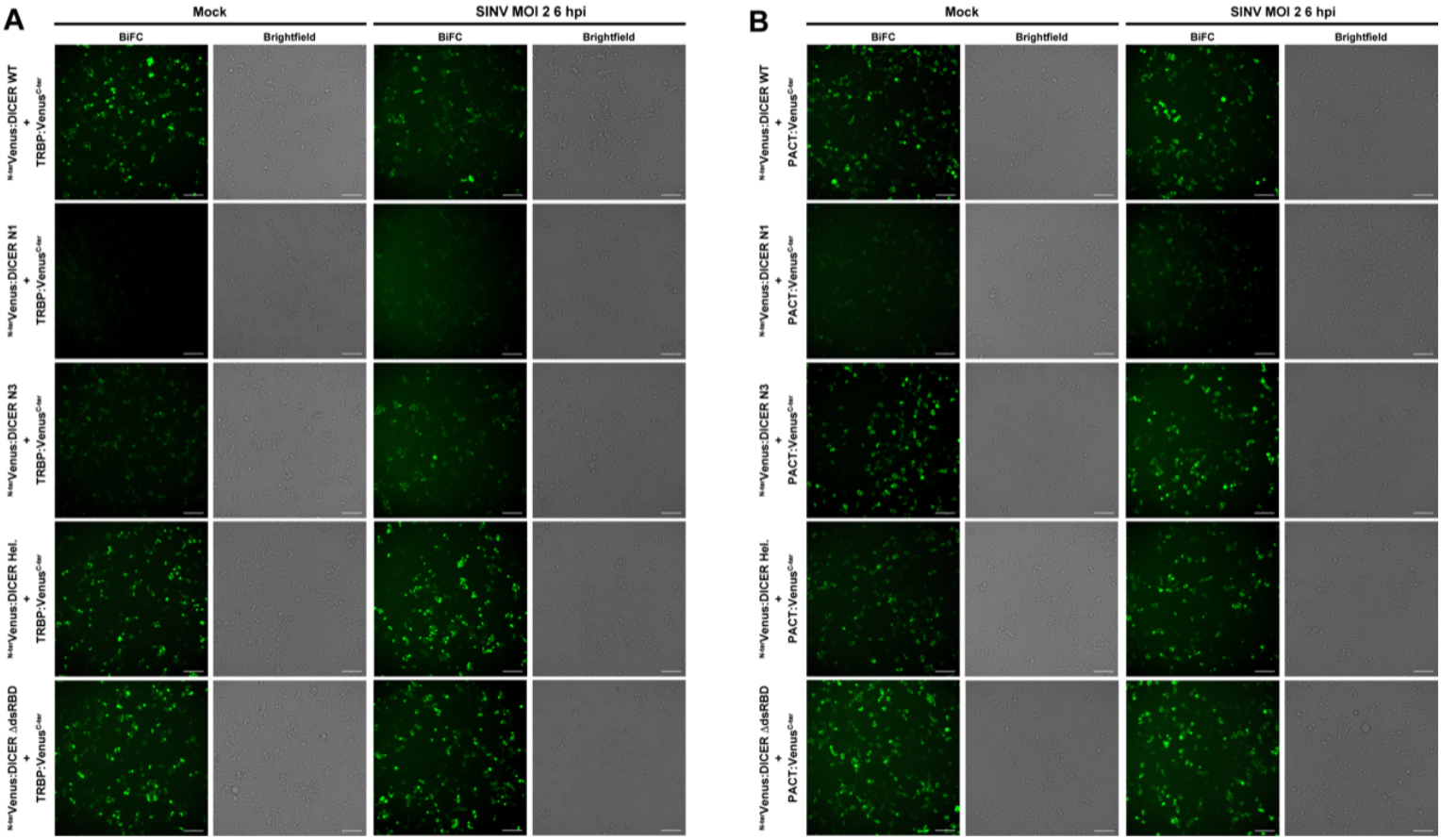

Figure S6